Weyl Disk Qubit

Quantum computation using the geometric phase in a four-terminal Josephson junction

by

Victor Boogers

to obtain the degree of Master of Science
at the Delft University of Technology,
to be defended publicly on Wednesday February 26th, 2020 at 15:00.

Student number:	4009436	
Project duration:	December, 2018 – February, 2020	
Thesis committee:	Prof. dr. Yuli V. Nazarov,	TU Delft, supervisor
	PhD student Janis Erdmanis,	TU Delft, supervising
	Dr. Anton Akhmerov,	TU Delft
	Prof. dr. Sander Otte,	TU Delft

TU Delft

Contents

1

Summary

Controlled quantum manipulation has been a dream of theoretical physicists and computer scientists since Feynman and Shor. At the moment there are multiple promising techniques to build qubits and construct a quantum computer, there are for example the Andreev qubits [15–17], Majorana systems [7], atoms or ions in an optical lattice [3, 14], superconducting qubits [6]. The main goal of most systems is to achieve a noise level low enough to implement noise correction codes and make a reliable quantum computer. Noise is a manifestation of asymmetric coupling of the levels to the uncontrolled environment. However, in a degenerate subspace there is symmetric coupling to the environment and information encoded in the qubit has potential to persist longer. For instance, Majoranas are interesting for this reason. The Weyl disk also offers a degenerate subspace which has topological protection [29][30] and the question is whether it can form a viable qubit.

The Weyl disk quantum system can traverse cyclic evolutions, meaning initial and final states differ by only a phase factor. This phase is determined by the form of the trajectory. This is an example of holonomic computation, which has raised quite some interest for its insensitivity to the noise in the trajectory to first order and for its high resistance to dynamical noise [26].

Practical issues are initialising to a certain state and reading out. They could be performed with existing methods for the Andreev qubit of [17], if we would split the levels. By moving far away from the disc centre the degeneracy is broken. First an even and odd eigenstate emerge, then a ground and excited harmonic. Another way to split the levels is by going off of the disc in the easy direction.

For simplicity, we are focusing on an isotropic disc. In chapter 4 we give an analytical solution for the evolution on circular trajectories centred on the Weyl disk in formula (4.18) for the adiabatic case and formulas (4.21) and (4.22) for the nonadiabatic case using Moore's derivation [31]. We find that the connection is proportional the σ_z-operator.

In Chapter 5, we numerically investigate our system using the exact formulas and assess the ability to do holonomic computation with circular trajectories. First, we reproduce the results of the Weyl disk paper to be sure that we are considering the correct limit (figure 5.1). Then we show our wavefunctions are localized in the minima and isolated from each other and are coming closer as we move away from the centre of the disc (figure 5.2). The main result is the σ_z-operator projected on the two states in the minima shown in figure 5.3. We see that the spins of the levels are aligning with the disc as we move away from the centre, which results in different geometric phases. In the same figure numerical convergence is proved.

In Chapter 6 we simplify the workings of our system in quasi-classical limit by using the strong localisation of the states in the phase space. We assume that wavepackets are in the classical minima and that quasi-spins are always opposite to the phases, as shown in figure 6.2. We test latter property numerically in figure 6.3, which shows good agreement. We then calculate the connections for moving radially and tangentially (eqs. (6.26), (6.30)) and find that only the tangential direction has non-zero connection and only gives a phase as before.

In chapter 7, we calculate geometric phases for different trajectories in the approximations of chapter 6. We show in figure 7.2 that as long as the trajectory encompasses the centre of the disc there is a geometric phase only determined by the enclosed area for small values of this area. Insignificance of the form of the trajectory proves fluctuations in parameter space do not affect the geometric phase to

first order. To test our method we compared the geometric phase in our quasi-classical approach to the result of chapter 5 and see in figure 7.1 that for large quasi-classical parameter it does approach the quasi-classical solution.

In conclusion, we are proposing a new kind of qubit for a multiterminal superconducting junction with a Weyl point, which is softened with a linear circuit. We show that within the degenerate subspace holonomic computation is possible and is insensitive to fluctuations of the trajectory. Further research is needed to make general qubit manipulation possible.

2

Introduction

2.1. Quantum computing

2.1.1. History

Since the discovery of the Turing machine in 1936 (a ”model of a computer” proposed by Turing) people have been wondering whether there are algorithms performed faster by some other system. Already in 1982 Feynman had a paper published about quantum computation, which was partly inspired by the difficulty of simulating quantum mechanics on classical computers [1]. This might be considered the start of quantum computing. In the early 1990's it was shown by several researchers that simulating quantum systems can be done efficiently on systems exploiting quantum physics. The most famous example is that in 1994 Shor demonstrated that two problems, finding prime factors for an integer and the discrete logarithm problem, are efficiently solved by quantum computers [2]. These problems have an interesting application in public key cryptography, where prime-factoring can be used to find the private key and crack the code. However, they do not yet have an efficient algorithm on a classical computer. This is one of the problems that reveal that quantum computers have some advantages over classical ones.

This can also be considered part of the field of quantum communication. Next to the above-mentioned cracking of public keys there are other applications such as communicating using entangled quantum states containing information. States are moved from A to B by entanglement, thereby teleporting a quantum state from one system to the other, while making it impossible to eavesdrop on the channel which would disrupt the signal.

The field of quantum information is rapidly growing. Firstly, because of the promises it brings for solving computational problems with fast algorithms, for applications in artificial intelligence, for quantum communication and for other fields. Secondly, because of the limitations that now arise in the fabrication of classical computers. For decades Moore's law has remained valid and the computational power approximately doubled every two years. But now dimensions have become so (microscopically) small that quantum mechanical effects make it hard to build ever smaller devices. The classical limits are near, whereas the quantum world sometimes seems unlimited in possibilities. Now scientists are exploring what is possible.

The promise of having a full-scale quantum computer has been driving the physics of quantum control in the field for the last two decades. At present, some small quantum computers have been built as a result. Often these are designed for a specific purpose, such as simulating heat transport through an atomic system as has been done by Harvard, MIT, CalTech [3]. More general quantum computing is still out of reach. Implementation of qubits and of means to probe those qubits is a present-day problem. Several challenges (treated in the next subsection) lie in creating robust systems fit for actual computation. That is why at present possibilities of making feasible systems are still limited and the state of the art systems only contain around 50 qubits of good quality (functional qubits, for instance, suffer less from noise).

Today only some quantum computing resources are available through the cloud and are accessed by research facilities. But several competitors are in the race of overcoming these obstacles and building more useful quantum computers, discussed in section 2.1.5

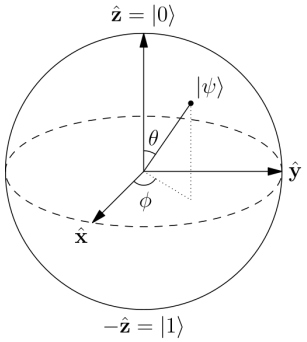

Figure 2.1: Bloch sphere. Every point represents a state of the form, where the overal phase is disregarded, because it is not important for quantum computation. [4]

2.1.2. Qubits

Qubits are the quantum analogue to classical bits. They are systems of two quantum states representing the ”0” and ”1”. Many candidates have been found by scientists for serving as qubits. The simplest example might be a spin-1/2 particle such as an electron, in which case the spin-up and spin-down states are used as ”1” and ”0”. As opposed to a classical bit, the qubit can be in a superposition of states. This changes the way of doing computation and brings new features and possibilities.

It is convenient in quantum information to map the state of a qubit onto the Bloch sphere, a unit sphere around the origin, where the bottom is the $|0\rangle$ state and the top is the $|1\rangle$ state (figure 2.1). The mapping is given by

$$(\theta, \phi) \rightarrow \cos(\theta/2)\,|0\rangle + e^{i\phi}\sin(\theta/2)\,|1\rangle\,, \tag{2.1}$$

where $\theta = 0..\pi$ and $\phi = 0..2\pi$. Manipulations of the state are SO(3)-operations (3D rotations around the origin) and so can be represented by rotations on the Bloch sphere. They are written as SU(2)-matrices. Some simple quantum logic gates interesting for computation are the phase gate R_ϕ adding a phase $e^{i\phi}$ to the $|1\rangle$ state, which is equivalent to a rotation around the z-axis on the Bloch sphere, the Pauli gates given by the Pauli matrices rotating by π around the corresponding axis, the Hadamard gate mapping the $|0\rangle$ and $|1\rangle$ states to respectively the mixed states $\frac{|0\rangle+|1\rangle}{\sqrt{2}}$ and $\frac{|0\rangle-|1\rangle}{\sqrt{2}}$. There are also multi-qubit operations such as the swap gate swapping the occupations of two levels. As an example of implementation, for the manipulation of the electron spin a magnetic field might be applied to rotate the spin around the field axis. For full quantum computation a *universal set of gates* is necessary, i.e. a set of gates from which all others can be constructed.

The important aspects of qubit systems are noise, control and scalability. One wants to be able to control the evolution of the qubit to implement quantum gates, i.e. to perform operations on it. Noise can interfere and complicate this. Think of fluctuations of the magnetic field strength or axis in the spin example. Finally, if a qubit allows for good computation, one would want to scale up to build computers of many qubits working together.

2.1.3. Superconductivity

A lot of qubits involve superconductivity. This is, simply put, the free movement of electrons without any resistance, which occurs at low temperatures in metals and also at higher temperatures up to over 130K in some exotic materials. This is caused by a pairing up of electrons into so called Cooper pairs.

Classically this can be explained as follows. Electrons in a conductor repell each other when they come close. Therefore one expects that electrons always want to be as far away from other electrons as possible. However, this doesn't take into account the interaction with the lattice of the metal. Electrons move through the lattice and interact with it, since the lattice has positive charge. The lattice is slightly deformed such that the electron is surrounded by some positive charge. This counters the repulsion between electrons with a attractive force, which can overcome the repulsion at long distances of typically hundreds of nanometers.

Superconductivity is, however, a quantum phenomenon and the rigorous treatment shows it is caused by electron-phonon interaction, where the phonon represents the collective motions of posi-

tive ions in the lattice. Cooper pairs consist of two fermions and are thus bosons and can occupy the same state. A certain range of the energy spectrum is condensed into a single state and this leaves an energy gap Δ. This is the binding energy of a pair and is in the order of millielectronvolts. This is easily overcome by temperatures that are not extremely low and superconductivity disappears if it is not cold enough. This energy gap also explains the absence of resistance, since exciting the fluid of cooper pairs costs an minimum of energy equal to the binding energy and this can not be paid at low temperatures.

2.1.4. Qubit experiments

What makes a feasible qubit? The answer was already mentioned in the last subsection. It depends on several aspects and is a careful trade-off between them. Every implementation has weaknesses, but the aim is to make a system functioning despite them. Here we elaborate on the characteristics and describe how they can be measured.

The most conclusive measurement of effective quantum manipulation is that of Rabi oscillations, oscillations between high occupation in either state, where the occupations vary as function of a rotation parameter. This is done by rotating on the Bloch sphere. For example, the spin of an electron can be rotated by a magnetic field, which is equivalent to a rotation on the Bloch sphere. The is what one would like to achieve to prove a system fit for operation.

A great obstacle is often the inevitable noise. There are several sources of noise. For instance, fluctuations can slightly alter the Hamiltonian and interfere with the evolution of the system. This could result in dephasing of the two states. In quantum computation there are ways to deal with noise and nonetheless achieve useful calculation. So-called quantum *error correcting code* can make for fault-tolerant quantum computation. However, this correction is only feasible above a certain noise threshold, which is often higher than the practical systems allow. Thus noise doesn't make computation impossible, but it should be minimised.

Two important quantities in this respect are the relaxation and coherence time. If there is an energy difference between the two states, the system will relax into the lowest state. Calculations have to be done in times much shorter than the relaxation time to produce useful results. The same holds for decoherence. States need to remain coherent, for also the phase is important in computation. If for example the energies of the levels slightly fluctuate, then the difference in dynamical phase could cause decoherence.

A measure for coherence time can be extracted from the Gaussian decay of so-called Ramsey fringes. Ramsey fringes are the oscillatory behaviour of the occupation of the levels after applying a $\pi/2$-pulse, waiting a time τ and applying a $\pi/2$-pulse again as function of the pause τ. So first the system is brought to an even superposition (on the equator of the Bloch sphere), then during the pause the qubit goes around the equator, and at some point it is rotated back along the same axis as before. This gives oscillatory behaviour as function of the pause length, but decoherence randomises the phases and results in a decrease in amplitude (figure 2.3).

2.1.5. State-of-the-art quantum computers

There are many systems eligible for qubit purposes. Most are solid state qubits, which involve electron transfers. Depending on the implementation, many quantities can provide the degree of freedom for the qubit, such as charge or superconducting phase or flux [5]. Consequently qubits can currently be made out of almost anything. The last decades lots of quite different systems have been competing in becoming the most promising technique. We list the most important developments. At IBM, Google, Intel and Rigetti superconducting circuit loops are used [6]. At QuTech in Delft scientists are currently working on a topological quantum computer [7]. Their qubits are topologically protected from noise, which gives a great advantage. They are using Majorana particles in a superconducting nanowire for this. IonQ manipulates trapped ytterbium ions with lasers and remarkably do that at room temperature [8]. The company D-Wave Systems uses a very different technique called quantum annealing to do calculations with thousands of qubits, which is already being used, but has not yet beaten classical computers [9]. Xanadu is also working on a room-temperature system based on photon states [10].

Some qubit systems are quantum simulators, meaning they only simulate a certain quantum system and are not for general purpose. Several quantum simulation problems have been proposed [11–13]. We give two examples of simulators. Within the team Harvard, MIT and CalTech atoms are trapped in an optical field and manipulated by using lasers [3]. They exploit the highly excited Rydberg states of

the atoms. In Maryland a group has been working on something similar also with an optical lattice, but they use trapped ions instead and the hyperfine states of the spins [14].

In spite of great efforts from many parties, a qubit reliable for large scale quantum manipulation has not yet been found. Recently Andreev bound states have been studied for qubit purposes and they could be an answer to the current issues [15–17]. In the present paper we treat a topological qubit based on Andreev levels, which should also be protected from noise.

2.1.6. Andreev qubit

Now it is time to get more specific about the subject of this thesis. We want to make an Andreev qubit. It uses two Andreev bound states (ABS), quasiparticle states in a normal region between two superconducting materials, also known as a Josephson junction. These states emerge as follows. At the barriers between the superconductor and the scattering region something called Andreev reflection can take place: if an electron in the scattering region has insufficient energy to enter the superconductor, it is reflected back as a hole. This implies charge transfer between the scattering region and the superconductor and implies the creation of a Cooper pair. This supercurrent is called Josephson current. Vice versa for a hole meeting a barrier. If the electrons/holes have insufficient energy to go to either superconductor, this constitutes bound quasiparticle states giving rise to a discrete energy spectrum and quasiparticles called Bogoliubons. Each transport channel in the scattering region gives rise to an Andreev bound state. Its energy depends on the transmission of the channel and the superconducting phase difference between the two superconductors. One can tune the ABS with these parameters to achieve a desirable qubit system.

Andreev level qubits have recently been an active subject of study. Often ABS are created using a weak link, which is a short region where superconductivity is weakened or broken and where the Josephson effect can take place. In 2002 a group proposed a system using a quantum point contact (QPC) in a superconducting ring to create ABS, where the QPC acts as a quantum dot [15]. The Andreev levels are coupled to the persistent Josephson current in the ring, which (through magnetic flux) can be measured to read out the Andreev qubit or can be used to manipulate the qubit. Also in 2002 others have suggested using the ABS levels in a SINIS-junction (superconductor - insulator - normal metal - insulator - superconductor) and controlling these by means of the voltage across one of the barriers and a separate transport current [16].

More recently an experiment has been done on an Andreev level qubit, demonstrating impressive features [17]. Their setup is a superconducting aluminium loop with a weak link in the form of an atomic contact. They created the contact using the micro-fabricated break-junction technique: the aluminium loop with a narrow constriction is put on a controllably bendable substrate, the substrate is bent until the bridge breaks, and further bending allows tuning of the transmission probability of its channels. The ABS spectrum has a ground and excited state and two intermediate states, which they show don't interfere. Tuning is done using a magnetic field: the magnetic flux through the loop determines the phase drop across the contact through $\delta = 2\pi\phi/\phi_0$ with ϕ_0 the flux quantum. An inductively coupled microwave resonator is employed to excite and probe the qubit through spectroscopy (figure 2.2).

Some of the results they have produced are Rabi oscillations and finding the relaxation and coherence time (figure 2.3). The coherence time is measured by looking at Gaussian decay of the Ramsey fringes. *The short coherence time was found to be caused by fluctuations of the energy levels, which in turn depends on the magnetic flux and the transmission.* Fluctuating transmission can be the result of mechanical vibrations or motions of the atoms close to the contact. The conclusion of the paper is that it is a proof of concept, but further investigation is needed into the sources of decoherence and scalability.

2.2. Holonomic quantum computation

Lately a new technique has enjoyed some attention for it's desirable features and notably it's resistance to noise. It employs the phase a system acquires by moving around a loop in parameter or projective Hilbert space. There have been already quite some proposals for physical systems implementing this geometric phase [18–22].

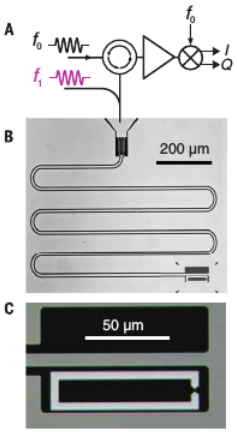

Figure 2.2: Setup for Andreev qubit. A loop with a weak link (C) is coupled to an inductively coupled microwave resonator (B). This in turn is probed by reflectometry (A). [17]

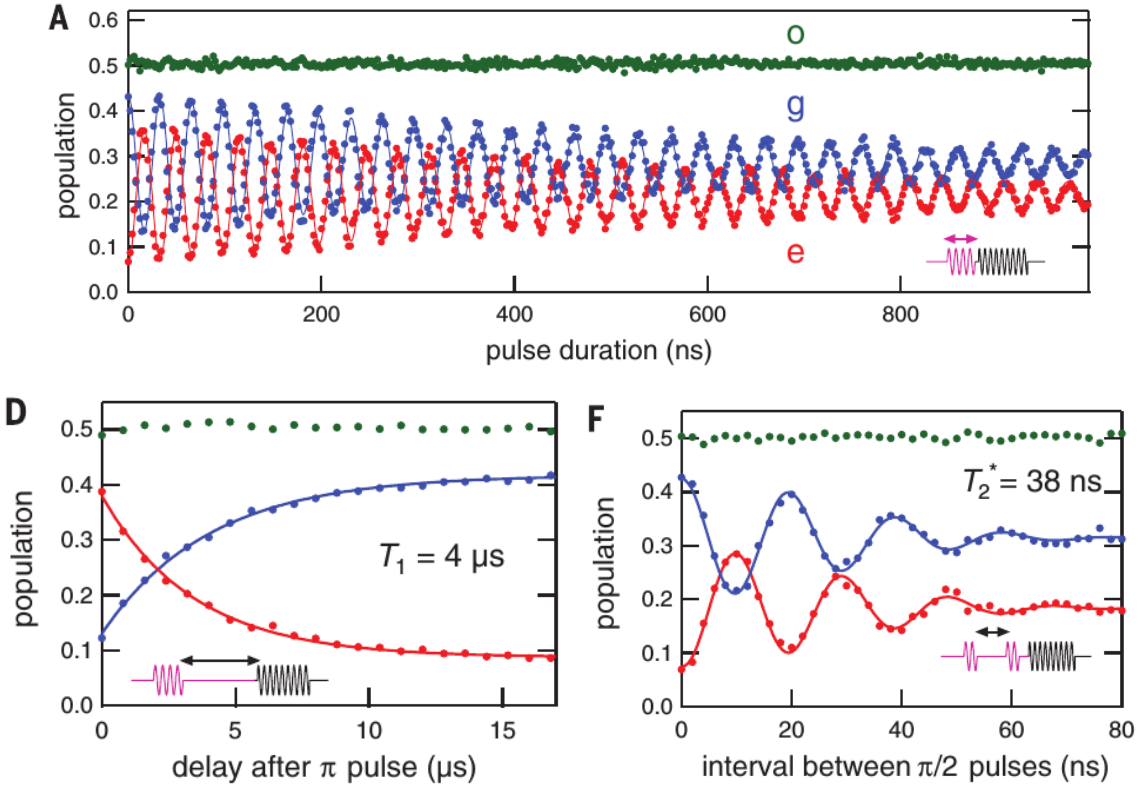

Figure 2.3: Red line indicates the excited state, blue line the ground state and the green line the intermediate states (which are parasitic and not part of the qubit). Plot *A* shows Rabi oscillations, plot *B* relaxation and plot *C* Ramsey fringes measuring coherence time. The short coherence time is blamed on fluctuations of Andreev levels. [17]

2.2.1. Geometric phase

Let's say that a Hamiltonian is a periodic function of time and that there are one or more states that undergo cyclic evolution, i.e. the state has only acquired a phase factor at the end of the period. Then these states are called cyclic states and their acquired phase consists of a dynamical and a geometric part. The dynamical phase is due to the energy of the system, but the geometrical phase depends on the path the state follows in Hilbert space. It is therefore considered a property of the spatial geometry.

To see how this geometric phase appears, consider Schrödinger's equation for time-dependent and periodic Hamiltonian, so $H(\tau) = H(0)$ [23].

$$H(t)\,|\psi(t)\rangle = i\hbar\frac{d}{dt}\,|\psi(t)\rangle \tag{2.2}$$

Take $\psi(t)$ normalised and cyclic such that $|\psi(\tau)\rangle = e^{i\phi}\,|\psi(0)\rangle$ with ϕ real. Now define $|\tilde{\psi}(t)\rangle = e^{-if(t)}\,|\psi(t)\rangle$ such that $f(\tau) - f(0) = \phi$ and so $|\tilde{\psi}(\tau)\rangle = |\tilde{\psi}(0)\rangle$. Filling in in (2.2) gives

$$\frac{df}{dt} = -\frac{1}{\hbar}\,\langle\psi(t)|H(t)|\psi(t)\rangle + \langle\tilde{\psi}(t)|i\frac{d}{dt}|\tilde{\psi}(t)\rangle \tag{2.3}$$

Now using this and defining the geometric phase as the total phase minus the dynamical phase,

$$\beta \equiv \phi + \int_0^\tau \langle\psi(t)|H(t)|\psi(t)\rangle\,dt, \tag{2.4}$$

it follows that

$$\beta = \int_0^\tau \langle\tilde{\psi}(t)|i\frac{d}{dt}|\tilde{\psi}(t)\rangle\,dt \tag{2.5}$$

Now consider the projective Hilbert space $\mathcal{P}$, that is the image of a map, mapping states differing only by a complex phase to the same element. For every curve $\tilde{C}$ in $\mathcal{P}$, which is the projection of the curve C traversed through the Hilbert space $\mathcal{H}$, we can choose a function $f(t)$ such that we get the same $\tilde{\psi}(t)$ and thus the same β. Also (2.5) shows that β is independent of parameter t. It can be concluded that β is a geometric property of the curve $\tilde{C}$ in $\mathcal{P}$ only.

Now consider the adiabatic limit, i.e. we change our Hamiltonian slow enough such that if a wavefunction is in an eigenstate it stays in the (moving) eigenstate [24]. In adiabatic evolution the cyclic states are thus eigenstates of the Hamiltonian. If we plug those in (2.5), we obtain the formula for Berry phase. A visual picture of this phase comes from rewriting this as a surface integral over the Berry curvature in parameter space [25], if we consider the time dependence of the Hamiltonian through some parameters $\vec{R}(t)$

$$\beta = \int_0^\tau \langle m(t)|i\frac{d}{dt}|m(t)\rangle\,dt = \int_0^\tau \langle m(t)|\nabla|m(t)\rangle\,d\vec{R}(t) = \int_A \langle\nabla m(t)|\times|\nabla m(t)\rangle\,dS. \tag{2.6}$$

In this thesis we are mainly interested in adiabatic evolution of the state within a degenerate subspace, where $H(t)\,|\psi\rangle = 0$ (zero point is arbitrary). The subspace is then spanned by cyclic states, each having a geometric phase factor. In this case dynamical phases are the same for each level, thus we neglect them. This allows us to obtain the unitary operator U known also as a holonomic transformation [23]:

$$U = \begin{bmatrix} e^{i\beta_1} & & \\ & \ddots & \\ & & e^{i\beta_n} \end{bmatrix} = \mathcal{P}\exp\int_0^\tau \begin{bmatrix} i\,\langle\tilde{\psi}_1|\dot{\tilde{\psi}}_1\rangle & & \\ & \ddots & \\ & & i\,\langle\tilde{\psi}_n|\dot{\tilde{\psi}}_n\rangle \end{bmatrix} dt, \tag{2.7}$$

where $\mathcal{P}$ is the path-ordered product operator, which is out of scope here. The matrix is called the connection M and we write

$$U = \mathcal{P}e^{\int_0^\tau M(t)dt}. \tag{2.8}$$

A simple 2×2 case is derived in appendix 9.1. We might want to use a different basis and wonder if we can adjust our connection to give the right result for our basis, but this is not easily done. The resulting

evolution operator should be the same as when we change basis afterwards. The integral prohibits simply transforming the connection to achieve this [1].

Holonomic computation has several benefits. The nonabelian Berry phase can be expressed as a line integral through the parameter space, but it is also possible to transform it into an integral over a surface enclosed by the loop using Stoke's theorem. This emphasizes the geometrical nature and means that the phase is almost only dependent on the area enclosed by the loop [26]. It also makes the qubit insensitive to random noise to first order in the driving of the evolution [26, 27].

Another benefit is that we can do computation in degenerate subspace. Thus the dynamical phase factor doesn't play a role any more. This is namely the same for both states. Any noise in this phase is therefore also absent [26]. However, adiabaticity constrains the time frame of computation [28]. Not only does this limit speed, but also becomes an issue when decoherence time doesn't exceed this time. For non-adiabatic evolution things are the other way around, fast evolution but with disturbence from dynamical phases.

Lastly, there is no energy relaxation between the levels, because they are degenerate and the relaxation process requires certain energy difference [26]. This excludes bit-flip errors (unwanted occupation changes).

[1] We can split the integral into infinitesimal parts $\int_0^\tau Mdt = \int_0^{t_1} Mdt + \int_{t_1}^{t_2} Mdt + \cdots + \int_{t_{n-1}}^{\tau} Mdt$ and approximate the exponent as $\exp(\int_0^\tau P(t)M(t)P^\dagger(t)dt) = P(0)\exp(\int_0^{t_1} Mdt)P^\dagger(0)\ldots P(t_{n-1})\exp(\int_{t_{n-1}}^{\tau} Mdt)P^\dagger(t_n - 1)$. We try to rewrite the transformation matrix products $P^\dagger(t_k)P(t_{k+1})$ using Taylor expansion of the second matrix as $(\mathbb{1} + P^\dagger(t_k)\frac{dP}{dt}\Delta t + \ldots)$. The second term should be zero to justify simply changing basis of the connection and then integrating.

3

System

3.1. Introduction to Weyl Disks

3.1.1. Multiterminal Josephson junction

It has recently been shown that multiterminal superconducting junctions (figure 3.1) with topologically trivial leads and without exotic materials can be tuned such that two levels cross at zero energy (relative to Fermi level) in the ABS spectrum and that they can be brought to a *Weyl point* or Weyl singularity [29]. This is a point in momentum space (in our case the superconducting phase ϕ takes the role of momentum) where two bands cross linearly (degeneracy). What is special about this point, is that it has topological protection, meaning in our case that any degeneracy is not easily lifted. The tuning parameters are the superconducting phases of the terminals, but due to gauge invariance one phase can be set to zero so the others span the parameter space.

Additionally, such Weyl point can be extended in two (or three) directions by coupling to external circuits, creating a *Weyl disks* [30]. The benefit of this all is a region, in which it is possible to move around without lifting degeneracy and even without fluctuations, making coherence time long. Our system is such a four-terminal Josephson junction with a nanostructure in the centre which exhibits a Weyl disk with nearly degenerate levels. It is mentioned at the end of the paper [30] that the Weyl disk system is interesting because of the possibilities for quantum computation. We intend to investigate if this system could establish a qubit.

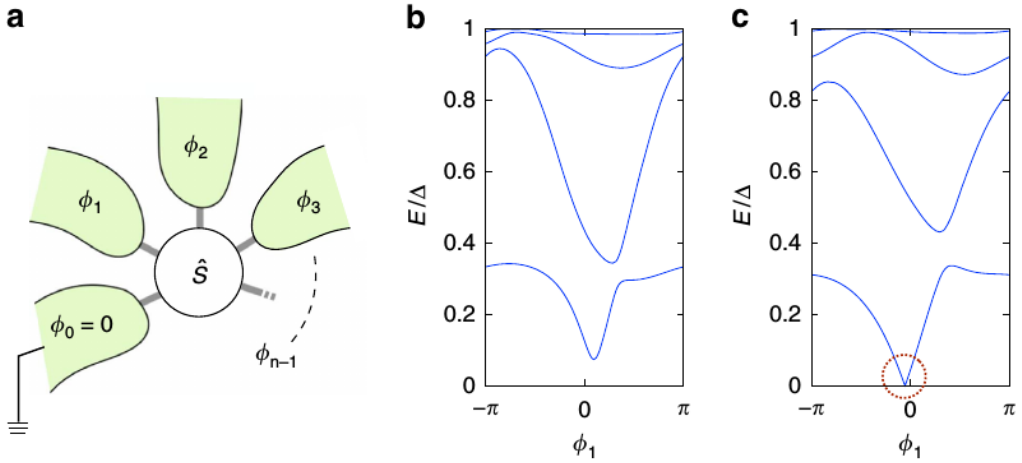

Figure 3.1: *Left*: Multiterminal superconducting junction with superconducting phases ϕ_n. *Middle*: The spectrum as function of ϕ_1 with the other reservoir phases away from the Weyl singularity. Δ stands for the superconducting energy gap. *Right*: The spectrum tuned by means of reservoir phases to the point of an energy level crossing. [29]

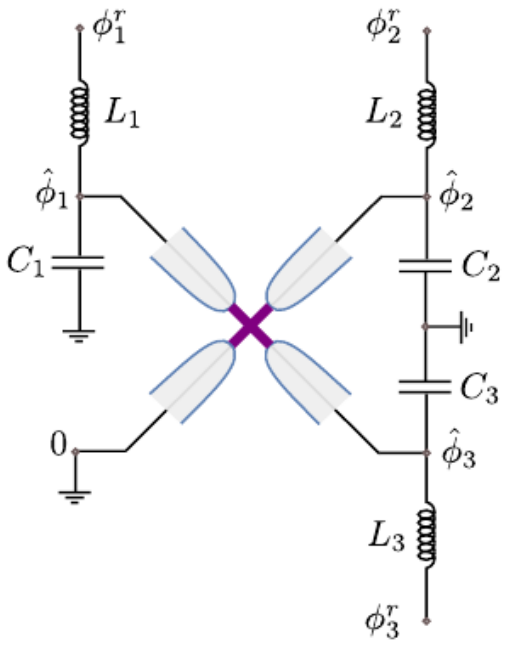

Figure 3.2: Model of the four-terminal Josephson junction in a realistic environment. The contacts have certain capacity and the superconducting leads have inductances, which are modeled in the circuit. [30]

3.1.2. Four-terminal Josephson junction with soft constraint

We should look first at the Hamiltonian to understand the dynamics and, in order to find it, the behaviour of the phase parameters must first be explained. They aren't fixed numbers (hard constraint) in a realistic setup, but are susceptible to backaction from the system and fluctuations and are therefore dynamical quantum variables [30]. This constitutes a *soft constraint*. To model this scenario an energy term of the form $(\hat{\phi} - \phi^r)^2/2L$, where ϕ is a superconductor phase and L is a inductance, is added to the Hamiltonian pulling the operator $\hat{\phi}$ towards the value ϕ^r, together with a charge term $\hat{Q}^2/2C$, where $\hat{Q}$ is the charge operator and C a capacitance, accounting for the fluctuations of $\hat{\phi}$.

The system is embedded in a linear circuit to account for the adjusted dynamics just discussed. Naturally the inductivity provides a soft constraint and the capacitances provide fluctuations (figure 3.2). The phases in the nanostructure are softly constrained to the phases of the leads, determined by the superconducting loops used to set the phase differences between the leads. When this is done, the Weyl point (in the phase space of the nanostructure) spreads out over a two-dimensional disc in the space of reservoir phases ϕ_n^r (figure 3.3).

Now we can build the Hamiltonian. Around the Weyl point it is effectively $H_{WP} = (\hbar/2e)\sum_{n=x,y,z} I_n \hat{\phi}_n \hat{\sigma}_n$, where $\hat{\sigma}_n$ are the Pauli matrices in the space of ground and excited singlet states, I_n are the coefficients of the linear crossing and $\hat{\phi}_n$ is the superconducting phase relative to the Weyl point. The full Hamiltonian also considering the soft constraint is

$$H(\vec{\phi^r}) = \frac{\hbar}{2e}\sum_{n=x,y,z} I_n \hat{\phi}_n \sigma_n + \left(\frac{\hbar}{2e}\right)^2 \frac{(\hat{\phi}_n - \phi_n^r)^2}{2L_n} + \frac{\hat{Q_n}^2}{2C_n}, \tag{3.1}$$

where the middle term accounts for the soft constraint and the last term for the fluctuations. The system can be better understood when one considers only one dimension. Then the Hamiltonian and quasi-spin can be diagonalised simultaneously so that we can write the kinetic part ("ϕ-part") as $(\hat{\phi} - \phi^r + \sigma IL)^2/2L - I^2L/2$. Classically there are two degenerate minima at $\phi^r - \sigma IL$ for the two quasi-spin values, separated by a barrier of height $E_B = LI^2/2$.

However, for this situation there exist two regimes. To distinguish between regimes, a quasi-

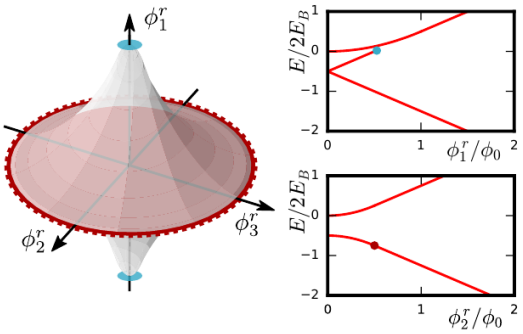

Figure 3.3: *Left*: Depiction of the Weyl disk system for (3.1). The surface is where three minima of the nanostructure exist. The red disc is where two minima become degenerate and is called the Weyl disk. (Parameters: $L_n = L/n, I_n = I$.) *Right*: The energy spectrum for varying the reservoir phase within the disc (above) and out of the disc (below). The reservoir phases are scaled with ϕ_0. [30]

classical parameter is defined

$$Q = \frac{1}{2}\left(\frac{LIe}{\hbar}\right)^2 \frac{\hbar}{e^2 Z}, \tag{3.2}$$

where $Z = \sqrt{L/C}$ is the characteristic impedance of the oscillator. This is the ratio of the barrier height to the oscillator energy quantum. If $Q \gg 1$, the states in the two minima don't notice each other and the system is in the quasi-classical regime. The states can be considered localised in this case and can be approximated by a harmonic oscillator for each quasi-spin value. For $Q \ll 1$ the opposite is true, and the coupling between the states makes quantum effects become stronger.

In the 3D case something similar happens. The minima are separated in the direction of largest $I_n^2 L_n$, which is called the easy-direction and corresponds to $n = 1$ in figure 3.3. The Weyl disk system will be considered in the quasi-classical regime, where the influence of soft constraint is well noticeable. Then we have a Weyl disk in the plane in directions $n = 2, 3$. It must be noted that there are two 3D spaces of the superconductor phases. One is the parameter space, the space of the reservoir phases ϕ_n^r. This is where the Weyl point is spread out over a disc. The other is the coordinate space, the space of coordinates ϕ_n corresponding to the operators $\hat{\phi}_n$, where the minima of the double-well potential are.

3.1.3. Weyl disk computation

Considering the possibility to make loops in the space of reservoir phases without breaking degeneracy of the ground states, it is interesting to see whether the Weyl disk system can be used for holonomic computation. It is possible to take advantage of the two lowest levels residing in the minima in coordinate space (space of ϕ_n) for qubit operation. The quasi-classical regime is needed, so the states do not couple too strongly and don't show unwanted interaction and perhaps become non-degenerate. We will namely consider only the adiabatic limit. The parameters in the Hamiltonian will be the external phases ϕ_n^r. By traversing a loop in the Weyl disk it is hoped that relative phase factors arise (rotation around z-axis of Bloch sphere). Then these could then be converted into arbitrary unitary operations (rotations) by measuring in a different basis. That might open the window to a variety of quantum gates.

There is the problem of reading out and setting up the state of the qubit. This could be done by moving to the outside of the disc, so the states will come together, couple and split or by moving in the easy direction off the disc and split the eigenspace into two levels each residing in one of the minima. Then probing or initialising might be done in a way similar to that in the previously discussed Andreev qubit system, coupling the levels to a resonator [17].

We may expect desirable behaviour from our qubit. Noise should play a much smaller role here than for the Andreev quantum dot and other systems. The holonomic/geometric nature of the manipulation and the topological protection of the Weyl point/disc account for this. By virtue of the degeneracy of the two qubit states, the dynamical dephasing is expected to be minimal, certainly since the degeneracy is topologically protected. The dynamical phase should be the same for both, and this would not alter the qubit state. The relaxation time depends on the separation in the parameter space. If the wave functions overlap, the quasi-particles spontaneously migrate from one state to the other. This means no difficulty in our case during manipulation, as we restrict ourselves to a degenerate level which excludes overlap since that would cause an energy splitting.

To verify our expectations, the behaviour of the qubit around the Weyl disk is assessed by both analytical and numerical results. The results presented here are valid in the regime $\Delta \ll \omega \ll \omega_0$, where Δ is the energy difference between the almost degenerate levels and ω_0 is the energy quantum in the spectrum of the coupled harmonic oscillator (as mentioned in the 1D example above) and ω is the frequency of the cycle through parameter space. This constraint guarantees that the levels interact with each other, but not with any higher levels thanks to adiabaticity.

4

Circular trajectory on isotropic disc

As a first experiment, the specific case of a circular trajectory through an isotropic disc (with the same centre as the disc) is examined. With isotropic we mean symmetric with respect to rotation around the easy-axis. This case is a simple example and is meant to give a basic understanding of the behaviour and possibilities of our system and help study more complex trajectories. We repeat the assumptions to emphasise the validit of our results. Everything is done in the quasi-classical regime $Q \gg 1$. To obtain a holonomic transformation, we restrict ourselves to the limit $\Delta \ll \omega \ll \omega_0$, where Δ is the level spacing between the nearly degenerate states and ω_0 is the harmonic oscillator level spacing.

In this thesis $\hbar$ and $2e$ are taken to be unity. The time-independent Hamiltonian for the Weyl disk is then given by

$$H(\vec{\phi}^r) = \sum_{n=x,y,z} H_n(\phi_n^r), \qquad H_n(\phi_n^r) = I_n\hat{\phi}_n\sigma_n + \frac{(\hat{\phi}_n - \phi_n^r)^2}{2L_n} + \frac{\hat{Q}_n^{\,2}}{2C_n}. \tag{4.1}$$

The external reservoir phases $\vec{\phi}^r$ are the parameters that are made time-dependent and will traverse a closed path through parameter space. The easy direction is taken to be along the z-axis by taking L_z and I_z larger than $L_{x,y}$ and $I_{x,y}$. The Hamiltonian can be split into two terms, involving the easy and the radial direction respectively, by setting $I_{x,y} = I_r$, $L_{x,y} = L_r$, $C_{x,y} = C_r$ (isotropy): $H = H_z + H_r$. The time-dependent Hamiltonian is

$$H(t) = H(R_z(t)\vec{\phi}^r) = H_z(\phi_z^r) + H_r(R_z(t)\vec{\phi}^r), \tag{4.2}$$

where $H_r(\vec{\phi}^r) = H_x(\phi_x) + H_y(\phi_y)$ and $R_z(t)$ is an operator rotating a vector by ωt around the z-axis.

4.1. Rewriting Hamiltonian

A cyclic state is a state which performs cyclic evolution as discussed in 2.2.1 about geometric phases. It is possible to find cyclic states in the adiabatic limit for the Weyl disk system, but for this the Hamiltonian will first be rewritten in the form $e^{-iAt}H(0)e^{iAt}$.

4.1.1. Rotation symmetry of the Hamiltonian

It will be shown that it is possible to rewrite (4.2) as two rotations, coordinate rotation and spin rotation. The rotation operators are then written as exponents. We start rewriting the Hamiltonian. Let the subscripts R/R^{-1} indicate that vectors are rotated by $R_z(t)/R_z^{-1}(t)$. Then we can write

$$\begin{aligned} H_r(t) = H_r(R_z(t)\vec{\phi}^r) &= I_r(\hat{\phi}_x\sigma_x + \hat{\phi}_y\sigma_y) + \frac{(\hat{\phi}_x - \phi_{Rx}^r)^2 + (\hat{\phi}_y - \phi_{Ry}^r)^2}{2L_r} + \frac{\hat{Q}_x^{\,2} + \hat{Q}_y^{\,2}}{2C_r} \\ &= I_r(\hat{\phi}_x\sigma_x + \hat{\phi}_y\sigma_y) + \frac{(\hat{\phi}_{R^{-1}x} - \phi_x^r)^2 + (\hat{\phi}_{R^{-1}y} - \phi_y^r)^2}{2L_r} + \frac{(\hat{Q}_{R^{-1}x})^2 + (\hat{Q}_{R^{-1}y})^2}{2C_r}. \end{aligned} \tag{4.3}$$

Note that the sum of the squares of the x- and y-terms does not change when rotated. Furthermore the first term in the last line is rewritten

$$I_r(\hat{\phi}_x\sigma_x + \hat{\phi}_y\sigma_y) = e^{-i\frac{\omega t}{2}\sigma_z}[I_r(\hat{\phi}_{R^{-1}x}\sigma_x + \hat{\phi}_{R^{-1}y}\sigma_y)]e^{i\frac{\omega t}{2}\sigma_z}. \tag{4.4}$$

Here the $e^{\pm i\frac{\omega t}{2}\sigma_z}$ rotate the quasi-spin operators around the z-axis over an angle ωt and is a well known operator in quantum information theory. The spin rotation cancels the phase rotation. After these observations our Hamiltonian can be written

$$H(t) = H\left(R_z^t\vec{\phi}^r, \vec{\hat{\phi}}, \vec{\hat{Q}}\right) = e^{-i\frac{\omega t}{2}\sigma_z}H\left(\vec{\phi}^r, R_z^{-t}\vec{\hat{\phi}}, R_z^{-t}\vec{\hat{Q}}\right)e^{i\frac{\omega t}{2}\sigma_z}. \tag{4.5}$$

At this point we have managed to prove that a rotation of the reservoir phases is equivalent to a rotation of the spins and a coordinate rotation (rotation of $\vec{\hat{\phi}}$ and $\vec{\hat{Q}}$).

4.1.2. Coordinate rotation operator

To reach our final form for the Hamiltonian, an operator is found for the rotations $R_z^{-1}(t)$. By rotating the coordinates $\vec{x} \rightarrow R\vec{x}$ and defining the operator $\tilde{U}(R)$ to rotate coordinates of the wavefunction $\tilde{U}(R)\psi(\vec{x}) = \psi(R\vec{x})$ it is possible to get from the eigen equation that

$$\tilde{U}(R)\vec{\hat{\phi}}\tilde{U}(R^{-1}) = R^{-1}\vec{\hat{\phi}}. \tag{4.6}$$

So we find that we can write the rotation of the phase operators using operators of coordinate rotation. The same can be done for $\vec{\hat{Q}} = i\vec{\nabla}$. It can be shown that $\vec{\nabla}' = R^{-1}\vec{\nabla}$. Remark that $\vec{\nabla}$ and $\tilde{U}(R^{-1})$ commute. These two properties are necessary to make the same calculation as before.

$$\tilde{U}(R)\vec{\hat{Q}}\tilde{U}(R^{-1}) = R^{-1}\vec{\hat{Q}}. \tag{4.7}$$

What remains is to find an expression for $\tilde{U}(R)$. In what follows the notation $\tilde{U}(\theta) = \tilde{U}(R(\theta))$ is used. For infinitesimal $\Delta\theta$ it holds that

$$\tilde{U}(\theta + \Delta\theta) = \tilde{U}(\theta) + \frac{\partial\tilde{U}}{\partial\theta}\Delta\theta. \tag{4.8}$$

If we fill in $\theta = 0$ we get the operator for rotation over infinitesimal angle

$$\tilde{U}(0 + \Delta\theta) = \mathbb{1} + \left.\frac{\partial\tilde{U}}{\partial\theta}\right|_{\theta=0}\Delta\theta. \tag{4.9}$$

This expression may be used to divide rotations into many small rotations

$$\tilde{U}(\theta) = \lim_{n\to\infty}\tilde{U}^n\left(\frac{\theta}{n}\right) = \lim_{n\to\infty}\left(\mathbb{1} + \left.\frac{\partial\tilde{U}}{\partial\theta}\right|_{\theta=0}\frac{\theta}{n}\right)^n. \tag{4.10}$$

The solution is a well known result in mathematics and reads

$$\tilde{U}(\theta) = e^{\left.\frac{\partial\tilde{U}}{\partial\theta}\right|_{\theta=0}\theta}. \tag{4.11}$$

We define $i\hat{L}_z = \left.\frac{\partial\tilde{U}}{\partial\theta}\right|_{\theta=0}$ and write $\tilde{U}(\theta) = e^{i\hat{L}_z\theta}$.

Putting everything together the final expression for the Hamiltonian is

$$H(t) = e^{-i\frac{\omega t}{2}\sigma_z}e^{-i\hat{L}_z\omega t}H\left(\vec{\phi}^r, \vec{\hat{\phi}}, \vec{\hat{Q}}\right)e^{i\hat{L}_z\omega t}e^{i\frac{\omega t}{2}\sigma_z} \tag{4.12}$$

or referring to our desired form

$$H = e^{-iAt}\tilde{H}e^{iAt} \tag{4.13}$$

with $\tilde{H} = H\left(\vec{\phi}^r, \vec{\hat{\phi}}, \vec{\hat{Q}}\right) = H(0)$ and $A = (\sigma_z/2 + \hat{L}_z)\omega$. Remark that only because σ_z and $\hat{L}_z$ commute it is possible to add them in one exponent.

4.2. Connection

4.2.1. Adiabatic

The Schrödinger equation for each of the degenerate eigenstates in adiabatic approximation is

$$H(\phi(t))\,|\pm(t)\rangle = e^{-iAt}H(0)e^{iAt}\,|\pm(t)\rangle = 0. \tag{4.14}$$

This expresses that at any time the eigenstate remains an eigenstate. We take the eigenenergy to be zero, because we are free to choose a null point. Since $H(0)\,|\pm(0)\rangle = 0$ it follows by substitution that

$$|\pm(t)\rangle = e^{-iAt}\,|\pm(0)\rangle \tag{4.15}$$

solves (4.14). Thus $U = e^{-iAt}$ is a holonomic transformation for circular trajectories. The $|\pm(0)\rangle$ are cyclic states.

With this solution we can evaluate the connection M_ϕ given by

$$U(t) = e^{-\int_0^\tau M(t)dt},\;\; M_\varphi(t) = \begin{bmatrix}\langle +|\dot{+}\rangle & \langle +|\dot{-}\rangle \\ \langle -|\dot{+}\rangle & \langle -|\dot{-}\rangle\end{bmatrix}. \tag{4.16}$$

We have given an index φ to the connection to indicate that only the angle on the disc changes during the (circular) trajectory. This will makes comparison later with section 6 clearer. Combining this equation with

$$|\dot{\pm}(t)\rangle = -iA\,|\pm(t)\rangle \tag{4.17}$$

we can evaluate connection M for circular closed trajectories in an isotropic disc, which is

$$M_\varphi = -i\begin{bmatrix}\langle +|A|+\rangle & \langle +|A|-\rangle \\ \langle -|A|+\rangle & \langle -|A|-\rangle\end{bmatrix}. \tag{4.18}$$

It turns out the components of $A = (\sigma_z/2 + \hat{L}_z)\omega$ have to be calculated for the evolution matrix. In the quasi-classical regime the minima both act as harmonic oscillators in the space of the ϕ, as will be become clear in figure 5.2 in the next chapter. This enables us to simplify even further, for we only expect ground harmonic oscillator states and can assess the L_z operator in this space. It can be derived, as done in appendix 9.2, that it is zero and can be discarded as long as this approximation holds. This means our operator is simply the quasi-spin operator $A = (\sigma_z/2)\omega$:

$$M_\varphi = -\frac{i}{2\omega}\begin{bmatrix}\langle +|\sigma_z|+\rangle & \langle +|\sigma_z|-\rangle \\ \langle -|\sigma_z|+\rangle & \langle -|\sigma_z|-\rangle\end{bmatrix}. \tag{4.19}$$

Also this is confirmed by calculations of chapter 5 in figure5.3. As we will see later, there are states in the minima which do not overlap, so (4.19) will be diagonal and these states are cyclic.

4.2.2. Nonadiabatic

A Hamiltonian of the form (4.13) has the solution

$$U(t) = e^{-iAt}e^{-iBt}, \tag{4.20}$$

where $B = H(0) - A$. This can be seen by direct substitution into the Schrödinger equation. An elaborate treatment is in appendix 9.3. In our case

$$U(t) = e^{-i(\sigma_z/2+L_z)\omega t}e^{-i(H(0)-(\sigma_z/2+L_z)\omega)t}. \tag{4.21}$$

This is the general solution to our problem. Below we simplify it for the limit we are considering, but otherwise it is the complete evolution operator. It should be applied when we are off of the disc or not in the Weyl disk limit and degeneracy is broken, or when we are moving too fast and higher levels come into play.

Equation (4.21) reduces to the previous adiabatic solution in the limit $\Delta \ll \omega \ll \omega_0$. Because $\omega \ll \omega_0$, the Hamiltonian $H(0)$ is much larger than $(\sigma_z/2 + L_z)\omega$, so we neglect the latter:

$$U(t) = e^{-i(\sigma_z/2+L_z)\omega t}e^{-iH(0)t} \tag{4.22}$$

The second exponent corresponds to the dynamical phase factor, which is irrelevant for nearly degenerate levels with $\Delta \ll \omega$, and thus the first exponent corresponds to the geometric phase factor. Here we can again choose to only consider ground state harmonic oscillator functions to drop L_z, as in previous subsection.

5

Numerical evaluation of the connection

Here we give some numerical results corresponding to the previous chapter characterising circular trajectories of the isotropic system in the quasi-classical regime. For convenience we do all calculations in the cyclic basis where one basis state is in the upper minimum and one in the lower minimum and from here on the states $|+\rangle$ and $|-\rangle$ respectively will denote these states. A very small offset is used ($\phi_z^r = 0.001$) for the calculations on the qubit to ever so slightly break degeneracy, so it is possible to get the wanted cyclic eigenstates easily by means of an eigensolver. We approximate the infinite dimensional Hilbert space by harmonic oscillator functions for each dimension.

We make sure we are in the correct limit by reproducing the energy spectrum of the Weyl disk paper [30]. To see whether the states are localised in superconducting phase space due to quasi-classics, we plot the wavefunctions. Finally we present the most important result, the geometric phase for different radii and the σ_z-operator responsible for this phase, and test this for convergence.

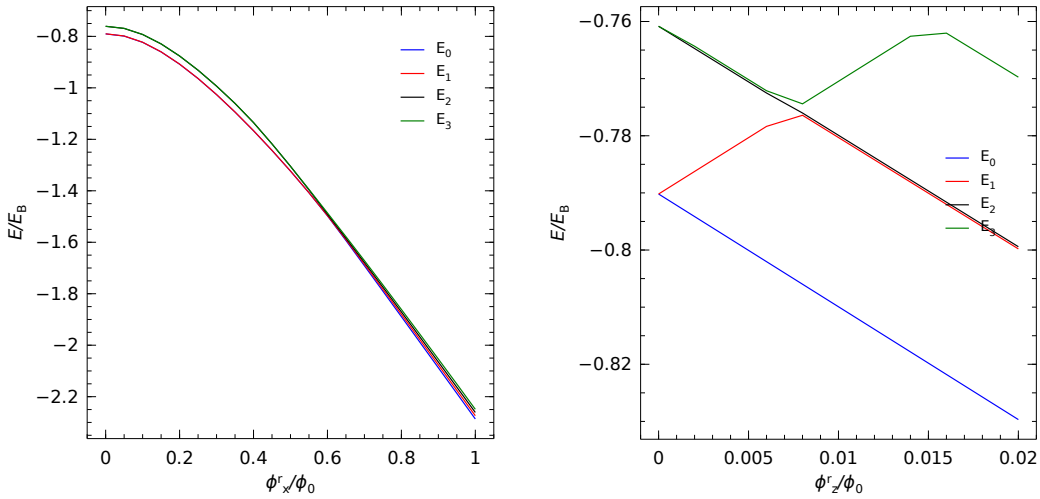

Figure 5.1: The first four energy levels of (4.1) as function of the radius of the circular trajectory on the disc (*left*) and offset of the circular trajectory from the disc (*right*) in phase space. The degeneracy of the eigenenergies which form the Weyl disk is reproduced. The right plot also shows that the levels can be split for measurement and initialisation. (The number of harmonic basis functions used is 20^3. Parameters are $L_z = 4, L_r = 4/3, C_n = 20, I_n = 1$.)

5.1. Numerical method

An eigensolver is used on the Hamiltonian in harmonic oscillator basis to calculate the eigenenergies, the probability density functions and the rotation on the Bloch sphere. This is done for different values of the reservoir phases. To examine the rotation on the Bloch sphere the radius on the disc is varied and then a rotation of the reservoir phases is simulated using the end result of the previous chapter, equation (4.22). The parameters for the Hamiltonian (4.1) are chosen $L_z = 4, L_r = 4/3, I_n = 1, C_n = 20$. Note that we do not have to constrict the range of the phases ϕ as we can scale them with the other parameters (I_n, L_n, C_n) to obtain the same results for smaller ϕ. For this reason the I_n can also be taken unity. The values for I_n create an isotropic disc and make the easy direction $n = z$. The capacities are taken large to be deep in the quasi-classical limit, however, as we will see later, convergence poses a restriction on this. In figure 5.1 the Weyl disk (shown in figure 3.3) is reproduced using these values. It shows the degeneracy remains for increasing radius and is lifted by creating an offset. This is needed so the levels remain degenerate and can potentially be initialised or read out by adding an offset.

5.1.1. Representing the connection

The evolution operator for the two lowest levels is calculated for the chosen parameters. It is verified to be unitary, which confirms our analysis. To investigate the unitary evolution operator as rotation on the Bloch sphere, notice that any unitary operator can be written $U = e^{i\gamma}e^{-i\alpha/2.\vec{\sigma}.\hat{n}} = e^{-i\alpha/2.\vec{\sigma}.\hat{n}+\gamma.1}$. Equations for the parameters in terms of our matrix elements are

$$U = e^{iA\tilde{t}} = \exp\left(i\begin{bmatrix} a_{11} & a_{12} \\ a_{21} & a_{22} \end{bmatrix}\right) = \exp\left(i\begin{bmatrix} -\alpha/2.n_z + \gamma & -\alpha/2.(n_x - in_y) \\ -\alpha/2.(n_x + in_y) & +\alpha/2.n_z + \gamma \end{bmatrix}\right), \tag{5.1}$$

where a_{ij} are the elements of $A\tilde{t}$. We want to extract the angle α from our matrix A. For the rotation axis direction $\hat{n}$ and rotation angle α the system of equations is

$$a_{12} + a_{21} = -\alpha n_x, \quad ia_{21} - ia_{12} = \alpha n_y, \quad a_{22} - a_{11} = \alpha n_z. \tag{5.2}$$

This is complemented with

$$\alpha = \sqrt{(\alpha n_x)^2 + (\alpha n_y)^2 + (\alpha n_z)^2}. \tag{5.3}$$

Then α is determined by

$$\alpha = \sqrt{(a_{12} + a_{21})^2 + (ia_{21} - ia_{12})^2 + (a_{22} - a_{11})^2}. \tag{5.4}$$

5.2. Results

5.2.1. The ground states

Figure 5.2 shows the two lowest states in the plane of the disc for different distances from the centre. They are localised and separated states. The further away from the centre of the disc, the more the wavefunctions of the lowest states move towards each other, and the weaker the localisation becomes. At some point the wave functions start to overlap. The plots are interpreted as indicating a double-well potential, meaning two wells separated by a barrier. The barrier lowers by moving away from the centre, which makes the wavefunctions approach each other. If the minima are close enough, an even and odd state emerge. Eventually the minima seem to join together (as we will see later in the quasi-calassical approach in figure 6.1), because a ground and excited harmonic state can be recognised. These states could be utilised to initialise and read out the qubit or form the basis of the qubit.

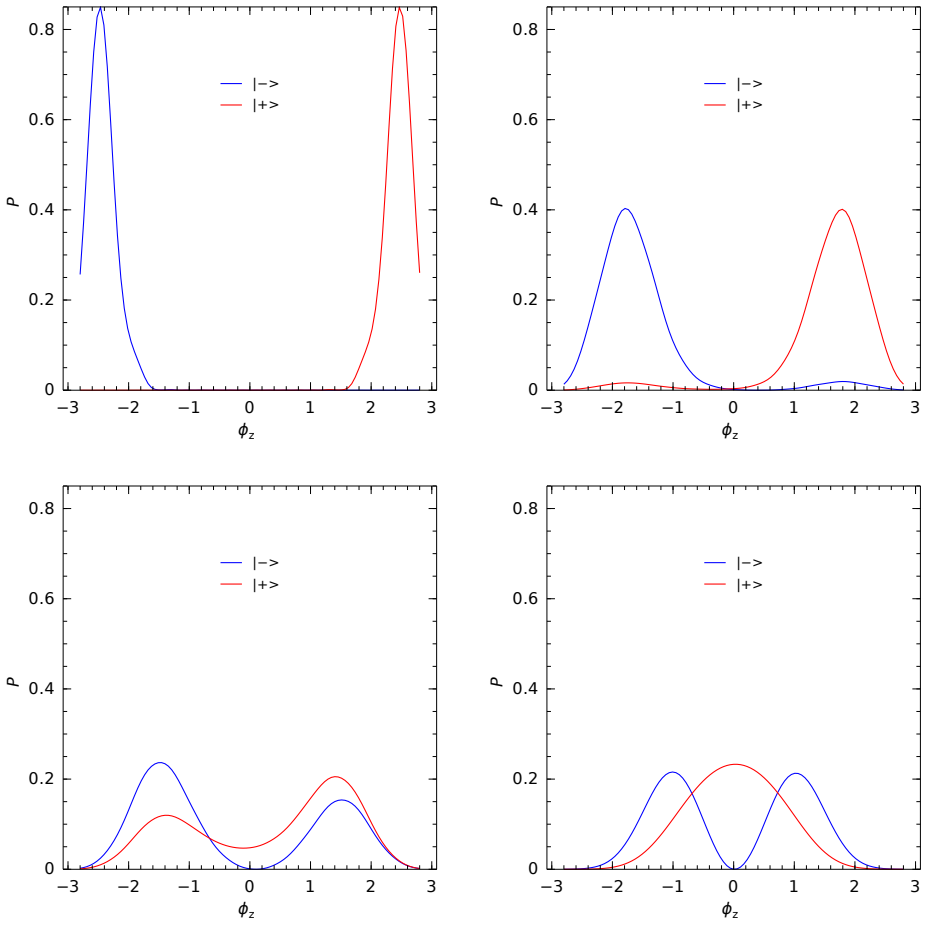

Figure 5.2: The probability function $P(\phi_z)$ for the two lowest levels of (4.1). *Top left*: $\phi_x^r = 0$, *Top left*: $\phi_x^r = 2$, *Top left*: $\phi_x^r = 2.2$, *Top left*: $\phi_x^r = 2.6$. The ϕ_y^r is always takn to be zero. The wavefunctions are quite localised, but move towards each other and become broader when moving away from the disc centre. They first form an even and odd state and later two harmonic states. (The number of harmonic basis functions used is 20^3. Parameters are $L_z = 4, L_r = 4/3, C_n = 20, I_n = 1.$)

5.2.2. Connection

The calculations show our chosen states are cyclic and only obtain a geometric phase without occupation changes. In figure 5.3 the geometric phase and in figure 5.4 the quasi-spin in the z-direction are displayed. The geometric phase follows precisely the quasi-spin of the two levels, as expected from equation (4.19). Our hypothesis that our qubit states are harmonic oscillator ground states, so the L_z-operator doesn't couple them, seems right. Although there seem to be no non-diagonal elements in the connection, fortunately the angle over which is rotated increases with radius. This is due to the

spin following (the direction of) the parameter phases (which will be tested also in the quasi-classical approximations in 6.3). This allows for rotation over the Bloch sphere around the z-axis for these cyclic states.

To show that we have a good approximation of our eigenfunctions and Hilbert space, we have varied the number of harmonic basis functions in figure 5.4. We have done this for several capacities and show the result for two values. We see that only for small capacities (up to $C = 20$) we have good convergence. For larger values convergence is unsatisfactory, which is why the value $C = 20$ was chosen for all curves.

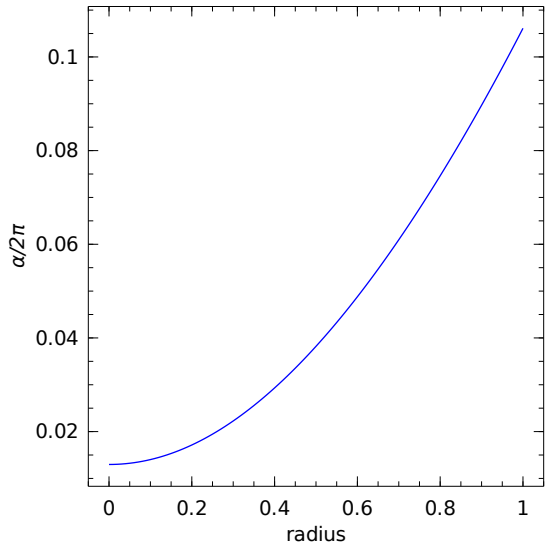

Figure 5.3: Plot showing the angle of rotation on the Bloch Sphere for traversing one cycle (*middle* and *right* respectively), all as function of the radius (of the circular trajectory). The Hamiltonian is (4.1). By varying the radius and possibly traversing multiple cycles any phase could be acquired. (The number of harmonic basis functions used is 20^3. Parameters are $L_z = 4, L_r = 4/3, C_n = 20, I_n = 1$.)

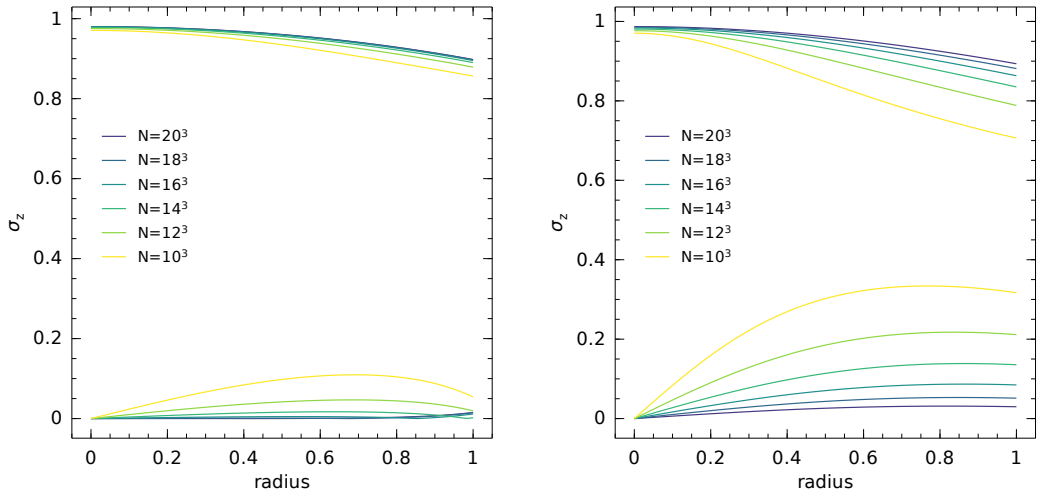

Figure 5.4: The expectation value of the σ_z-operator (*top* lines) and off-fiagonal terms (*bottom* lines). The number of basis states is varied for $C_n = 20$ and $C_n = 5$. There is convergence for $C_n = 5$ and $C_n = 20$, but for larger values it will be too slow. We see that spins of both levels are aligning with the disc as we move away from the centre. (Other parameters: $L_z = 4, L_r = 4/3, I_n = 1$.)

6

Quasi-classical approach for general trajectories

The aim in this chapter is to find a recipe for calculating the evolution matrix of any trajectory in the quasi-classical limit. We still consider an isotropic disc for simplicity. For general trajectories it is possible to find an expression for calculating the matrix M of (2.8) within the quasi-classical approach. We do this by separately considering the effects of moving in the radial and tangential direction. Consider a parameterisation of a trajectory $(r(t), \varphi(t))$ in the Weyl disk, where r and φ are the radius and angle in the x, y-plane. Using the chain rule, the time derivative is expressed by

$$\frac{d\,|\Psi\rangle}{dt} = \frac{\partial\,|\Psi\rangle}{\partial r}\frac{dr}{dt} + \frac{\partial\,|\Psi\rangle}{\partial \varphi}\frac{d\varphi}{dt}. \tag{6.1}$$

The derivatives $\frac{\partial|\Psi\rangle}{\partial r}, \frac{\partial|\Psi\rangle}{\partial \varphi}$ are needed to calculate arbitrary trajectories. We are looking for matrices $M_{r,\phi}$ that give us these derivatives

$$\frac{d\,|\Psi\rangle}{dt} = M_r\,|\Psi\rangle\,\frac{dr}{dt} + M_\varphi\,|\Psi\rangle\,\frac{d\varphi}{dt}, \tag{6.2}$$

in which case $M = M_r\frac{dr}{dt} + M_\varphi\frac{d\varphi}{dt}$. With these matrices we would be able to investigate any trajectory. We will evaluate these matrices as 2×2 in our qubit space, again for the $|\pm\rangle$ states.

To be able to calculate the dependence of the connection on our parameters, we need to make some simplifications first based on the quasi-classical limit. We make statements about the energy and the spin behaviour from a classical point of view.

We will again consider the Hamiltonian with reservoir phases somewhere on the plane of the disc and take again $I_n = 1$. We drop the charge terms, which as conjugate variables for the $\hat{\phi}$ make for a broadening of the wavefunction and are thus not influential here. This could be considered the limit of very large capacity. We put $\phi_x^r = r$ and $\phi_{y,z}^r = 0$ and write

$$H = \vec{\hat{\phi}}.\vec{\sigma} + \frac{(\hat{\phi}_x - r)^2}{2L_r} + \frac{\hat{\phi}_y^2}{2L_r} + \frac{\hat{\phi}_z^2}{2L_z} \tag{6.3}$$

6.1. Quasi-classical approach

Because we are in the quasi-classical regime, we can make two simplifications based on results of the previous chapter to predict the behaviours of our qubit. One concerning energy and the other concerning spin.

6.1.1. Energy condition

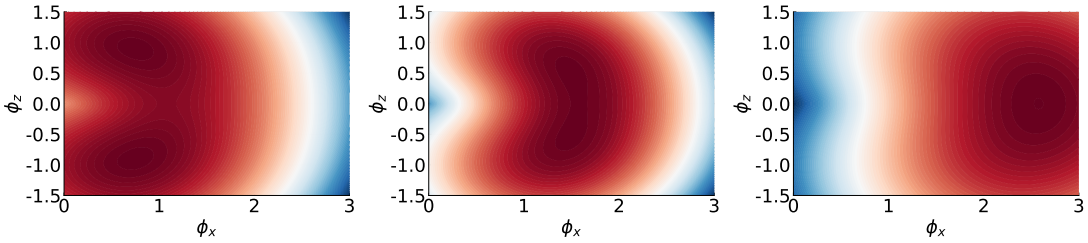

Figure 6.1: The potential of (6.4) in phase space for phase along the radial axis and z-axis. *Left*: $\phi_x^r = 0.5$, *Middle*: $\phi_x^r = 1$ *Right*: $\phi_x^r = 2$. The results in figure 5.2 that the wavefunctions should move towards each other for increasing radius on the disc are confirmed. (Parameters: $L_z = 4, L_r = 4/3$)

We have seen that the eigenstates have some classical behaviour in that they are localised and reside in the minima. A quasi-classical energy expression is therefore justified by replacing the operators $\hat{\phi}_n$ with their mean value ϕ_n and the quasi-spin part $\hat{\phi}_n\sigma_n$ with one of its eigenvalues $\pm\sqrt{\phi_n\phi_m}$ (for $\sigma = \pm 1$). What is left is

$$E_{cl,-} = -\sqrt{\phi_x^2 + \phi_z^2} + \frac{(\phi_x - r)^2}{2L_r} + \frac{\phi_y^2}{2L_r} + \frac{\phi_z^2}{2L_z}, \tag{6.4}$$

where we have substituted scalar E for the operator H in (6.3). For the minimum holds

$$\begin{aligned} \frac{\partial E}{\partial \phi_r} &= \frac{\phi_r - r}{L_r} - 2\phi_r \frac{1}{2\sqrt{\phi_r^2 + \phi_z^2}} = 0 \\ \frac{\partial E}{\partial \phi_z} &= \frac{\phi_z}{L_z} - 2\phi_z \frac{1}{2\sqrt{\phi_r^2 + \phi_z^2}} = 0. \end{aligned} \tag{6.5}$$

Beginning with the second line of (6.5) it is deduced that

$$(\phi_z = 0 \wedge \phi_r \neq 0) \vee L_z = \sqrt{\phi_r^2 + \phi_z^2}. \tag{6.6}$$

The solution with $\phi_z = 0$ corresponds to the maximum and is dropped. Using this in the first line of (6.5) we arrive at the expression for coordinate ϕ_r^0 of the minimum

$$\phi_r^0 = \frac{r}{1 - L_r/L_z}. \tag{6.7}$$

Inserting this in (6.6) gives the other coordinate ϕ_z^0

$$(\phi_z^0)^2 = L_z^2 - \left(\phi_r^0\right)^2 = L_z^2 - \left(\frac{r}{1 - L_r/L_z}\right)^2. \tag{6.8}$$

These are the coordinates of the two minima, where we will assume the cyclic wavefunctions reside. In figure 6.1 a 2D slice of the quasi-classical potential is displayed for three values of ϕ_x^r. It can be seen that the minima move towards each other for larger ϕ_x^r and eventually merge. The same can be seen in figure 6.2. It agrees with our earlier result in figure 5.2. There the wavefunctions also became wider, which can be explained by the vanishing of the barrier between the minima. As long as the barrier height is well above the ground state energy of the harmonic oscillators in the minima, the wavefunctions remain localised.

6.1.2. Spin condition

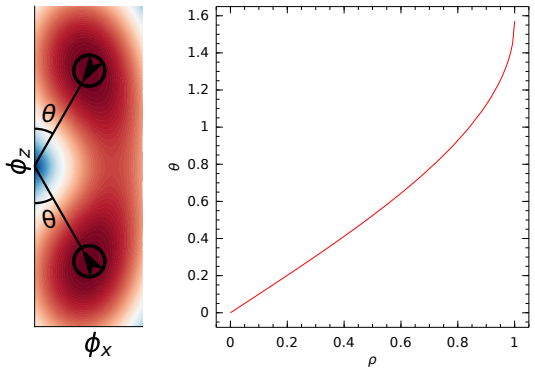

Figure 6.2: *Left:* The ϕ_x, ϕ_z-plane with the minima for opposite ϕ_z^0 and the spin vectors for the $|\pm\rangle$ states in opposite directions. The angle θ indicates how far off the direction of the minima is from the z-axis. *Right*: A plot of the angle θ versus the scaled radius on the disc $\rho = r/(L_z - L_r)$ made using (6.7) and (6.8). The relation is $\theta = \arcsin(\rho)$. Here it can also be seen from the angle $\pi/2$ at $\rho = 1$ that the minima merge in our quasi-classical approximation.

To minimise the energy term $\vec{\phi} \cdot \vec{\sigma}$ the spin is considered to be constrained to point in opposite direction to the minima, which are determined by the reservoir phases. This allows us to write

$$|\Psi\rangle\,(\phi_x, \phi_y, \phi_x^r, \phi_y^r) = \psi(\phi_x, \phi_y, \phi_x^r, \phi_y^r) \begin{bmatrix} s_+(\phi_x^r, \phi_y^r) \\ s_-(\phi_x^r, \phi_y^r) \end{bmatrix}. \tag{6.9}$$

Our assumption has been verified numerically to reasonable agreement in figure 6.3. The spin follows the phase vector closely and therefore we state the following spin condition. The position of the minima are written

$$\vec{\phi}_\pm^0 = \begin{bmatrix} \phi_x^0 \\ \phi_y^0 \\ \pm\phi_z^0 \end{bmatrix}, \tag{6.10}$$

where $\phi_z^0 > 0$. It is expected that the spin behaves as to minimise the first term of the Hamiltonian (6.3). The spin is then determined by the condition

$$\frac{\vec{\phi}_\pm^0 . \vec{\sigma}}{\left|\vec{\phi}^0\right|} |S\rangle = -|S\rangle \tag{6.11}$$

which we may also write as

$$(\cos(\pm\theta)\sigma_z + \sin(\theta)\sigma_x)\,|S\rangle = -|S\rangle\,, \tag{6.12}$$

where $|S\rangle$ is the spin of an eigenstate and θ is the angle the vector $\vec{\phi}^0$ makes with the positive z-axis clockwise (figure 6.2). This means the spin is antiparallel to the phase vector. This may be verified by filling in into (6.12) the spins

$$\begin{aligned} |S_+\rangle &= e^{i\sigma_y\theta/2}\,|\uparrow\rangle \\ |S_-\rangle &= e^{-i\sigma_y\theta/2}\,|\downarrow\rangle\,. \end{aligned} \tag{6.13}$$

Here the exponent rotates the quasi-spin and thereby our two levels over the Bloch sphere to anti-align them with the $\vec{\phi}^0$. The $|S_\pm\rangle$ states are the spins of the $|\mp\rangle$ states. By collapsing (6.12) and taking note of

$$\begin{aligned} e^{i\sigma_y\theta/2}\sigma_x e^{-i\sigma_y\theta/2} &= \cos(\theta)\sigma_x + \sin(\theta)\sigma_z \\ e^{i\sigma_y\theta/2}\sigma_z e^{-i\sigma_y\theta/2} &= \cos(\theta)\sigma_z - \sin(\theta)\sigma_x, \end{aligned} \tag{6.14}$$

we see that the equation is satisfied.

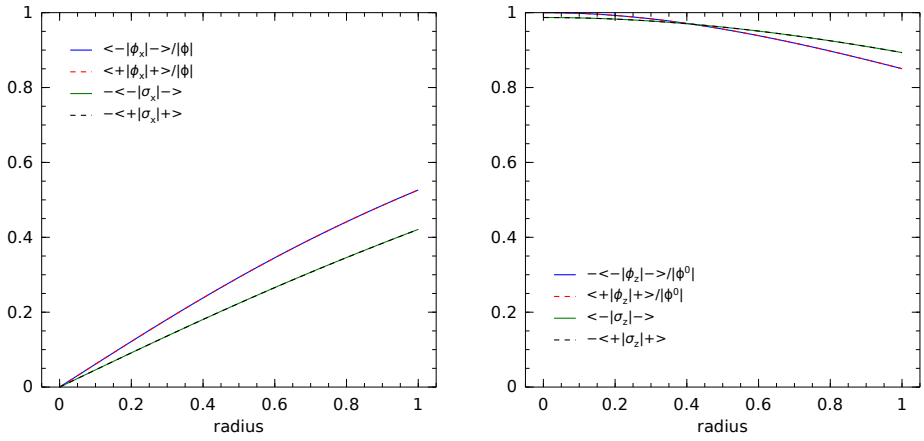

Figure 6.3: Comparison of the directions of the spin and of the phase in the minimum versus distance from the centre of the disc, assuming $\phi_y^r, \phi_z^r = 0$. The Hamiltonian is (4.1). *Left:* The radial components of spin and phase are *left* and the z-components are *right*. The spin follows the phase of the system, although not exactly, and so verifies the soundness of (6.11). (The number of harmonic basis functions used is 20^3. Parameters are $L_z = 4, L_r = 4/3, C_n = 20, I_n = 1$.)

6.2. Calculate M

The derivatives are calculated with the product rule to account for changes in the wavefunction and spin

$$\frac{d\,|\Psi\rangle}{dx} = \frac{d\psi}{dx}\,|S\rangle + \psi\frac{d}{dx}\,|S\rangle\,. \tag{6.15}$$

The term with derivative of the wave function $d\psi/dx$ doesn't contribute. To see this, collapse the term with $|\Psi\rangle$ and use partial integration. We have approximated the wavefunctions by only the ground state harmonic oscillator function in the respective wells, which is real and vanishes at infinity. Consequently, the outcome is real and we have no boundary term so that we can write

$$\langle\psi|\psi'\rangle = \int \psi^*\psi' d^3\phi = -\int \psi'^*\psi d^3\phi = -\langle\psi'|\psi\rangle = -\langle\psi|\psi'\rangle^*\,. \tag{6.16}$$

This represents the contribution to the matrix element of M_r and we may conclude that it has no real part and should thus be zero. Consequently only the spin derivative matters and we may write

$$\frac{d\,|\Psi\rangle}{dx} = \psi\frac{d}{dx}\,|S\rangle\,. \tag{6.17}$$

6.2.1. r-derivative

For the radial derivative we use the chain rule and (6.13), and obtain

$$\frac{d}{dr}\,|S_\pm\rangle = \frac{d\theta}{dr}\frac{d}{d\theta}\,|S_\pm\rangle = \pm\frac{d\theta}{dr}\frac{i\sigma_y}{2}\,|S_\pm\rangle\,. \tag{6.18}$$

The derivative $d\theta/dr$ can be expressed in coordinates of the minimum and consequently in the parameters. We use the chain rule

$$\frac{d}{dr}\cos\theta = -\sin\theta\frac{d\theta}{dr}, \tag{6.19}$$

and fill in the components of $\vec{\phi}^0$ (figure 6.2)

$$\begin{aligned}\phi_r^0 &= |\vec{\phi}^0|\cos\theta\\ \phi_z^0 &= |\vec{\phi}^0|\sin\theta.\end{aligned} \tag{6.20}$$

enabling us to express the derivative in coordinates of the minimum as

$$\frac{d\theta}{dr} = -\frac{d\cos\theta/dr}{\sin\theta} = -\frac{d\phi_z^0/dr}{\phi_r^0}. \tag{6.21}$$

To switch to parameter coordinates it is convenient to note that

$$\frac{d\phi_z^0}{dr} = \frac{-1}{1 - L_r/L_z}\frac{\phi_r^0}{\phi_z^0}, \tag{6.22}$$

so we finally arrive at an appropriate formula

$$\frac{d\theta}{dr} = \frac{1}{1 - L_r/L_z}\frac{1}{\phi_z^0}. \tag{6.23}$$

Substituting this in (6.18) we can write

$$\frac{d}{dr}\left|S_\pm\right\rangle = \pm\frac{i\sigma_y}{2\phi_z^0(1 - L_r/L_z)}\left|S_\pm\right\rangle = \pm\frac{i\sigma_y}{2\sqrt{(L_z - L_r)^2 - r^2}}\left|S_\pm\right\rangle. \tag{6.24}$$

This means we need to get the σ_y-matrix in our $|S_\pm\rangle$ basis, which turns out to be the same as in the quasi-spin basis. The components are readily evaluated to be

$$\begin{aligned}
\langle S_+|\sigma_y|S_+\rangle &= \langle\uparrow|e^{-i\sigma_y\theta/2}\sigma_y e^{i\sigma_y\theta/2}|\uparrow\rangle = \langle\uparrow|\sigma_y|\uparrow\rangle = 0\\
\langle S_-|\sigma_y|S_-\rangle &= \langle\downarrow|e^{i\sigma_y\theta/2}\sigma_y e^{-i\sigma_y\theta/2}|\downarrow\rangle = \langle\downarrow|\sigma_y|\downarrow\rangle = 0\\
\langle S_+|\sigma_y|S_-\rangle &= \langle\uparrow|e^{-i\sigma_y\theta/2}\sigma_y e^{-i\sigma_y\theta/2}|\downarrow\rangle = \langle\uparrow|\cos(\theta)\sigma_y - i\sin(\theta)\mathbb{1}|\downarrow\rangle = -i\cos\theta\\
\langle S_-|\sigma_y|S_+\rangle &= \langle\downarrow|e^{i\sigma_y\theta/2}\sigma_y e^{i\sigma_y\theta/2}|\uparrow\rangle = \langle\downarrow|\cos(\theta)\sigma_y + i\sin(\theta)\mathbb{1}|\uparrow\rangle = i\cos\theta.
\end{aligned} \tag{6.25}$$

The end result is the first matrix of equation (6.1), reading

$$M_r = \frac{1}{2\sqrt{(L_z - L_r)^2 - r^2}}\begin{bmatrix} 0 & -\cos\theta\,\langle\psi_-|\psi_+\rangle \\ -\cos\theta\,\langle\psi_+|\psi_-\rangle & 0 \end{bmatrix}. \tag{6.26}$$

For non-overlapping wave functions the connection in radial direction becomes zero.

6.2.2. Tangential derivative

The derivative w.r.t. φ is less involved. Our spin state as a function of φ is $|S\rangle = e^{i\sigma_z\varphi/2}\left|S\right\rangle_{\varphi=0}$, where as before the exponent rotates the spin. The derivative is

$$\frac{d}{d\varphi}\left|S\right\rangle = \frac{d}{d\varphi}e^{i\sigma_z\varphi/2}\left|S\right\rangle_{\varphi=0} = i\sigma_z/2\left|S\right\rangle. \tag{6.27}$$

This leaves the simple expression

$$\frac{d\left|\Psi\right\rangle}{d\varphi} = i\sigma_z/2\left|\Psi\right\rangle. \tag{6.28}$$

This is in agreement with the result (4.19) for isotropic circular trajactories. Now we calculate the connection. First we need to see that, using (6.14),

$$\begin{aligned}
\langle S_+|\sigma_z|S_+\rangle &= -\cos\theta\\
\langle S_-|\sigma_z|S_-\rangle &= \cos\theta\\
\langle S_+|\sigma_z|S_-\rangle &= \langle\downarrow|\sigma_z|\uparrow\rangle = 0\\
\langle S_-|\sigma_z|S_+\rangle &= \langle\uparrow|\sigma_z|\downarrow\rangle = 0.
\end{aligned} \tag{6.29}$$

At the last two lines we have used the definition of the exponent of σ_y and used that this commutes with σ_z. The result for the connection in tangential direction is

$$M_\varphi = \frac{i}{2}\begin{bmatrix} -\cos\theta & 0 \\ 0 & \cos\theta \end{bmatrix}. \tag{6.30}$$

This means that there will be no mixing, when moving in the tangential direction. However, an opposite phase factor is aqcuired by the states $|\psi_{\pm}\rangle\,|S_{\mp}\rangle$, which are recognised as cyclic. This phase will be vary for different trajectories, since there is a dependence on θ. This angle will change when r is varied as seen in section 6.2.2, or possibly also when the offset ϕ_z^r is changed as the minimum tends to follow the reservoir phases. We conclude that our results are in very good agreement with chapter 4 and 5.

Although there is no mixing in the cyclic basis, by taking a different measurement basis it is possible to rotate around a different axis on the Bloch sphere. This is how more general manipulations could become possible. For example, the even and odd states, $(|+\rangle + |-\rangle)$ and $(|+\rangle - |-\rangle)$, the rotation axis will lie on the equator and the phase of cyclic basis will be translated into only occupation changes. For the mentioned possible basis of ground and excited state another axis of rotation might become available.

7

Trajectories

Now that we have the quasi-classical connection, we can do some calculations with them for some simple trajectories. We have chosen the circle, which we already studied in chapters 4 and 5, a circle with the disc centre outside, on its edge and inside, an ellipse, and a square. We first give an analytical treatment of these examples and compare the results. Then we calculate the connections.

7.1. Parametrisation

To perform the integral of (2.8) it is needed to express the integrand $\cos\theta$ in φ. We make explicit the dependence on r, displayed in figure 6.2, and then $r(\varphi)$ is given per trajectory. The angle θ is determined by

$$\tan\theta = \frac{\phi_r^0}{\phi_z^0} = \frac{r}{\sqrt{(L_z - L_r)^2 - r^2}} = \left[\left(\frac{L_z - L_r}{r}\right)^2 - 1\right]^{-1/2}. \tag{7.1}$$

By using the relation

$$\cos(\arctan x) = \frac{1}{\sqrt{(x^2+1)}} \tag{7.2}$$

the integrand can be written as function of the parameter r

$$\cos\theta = \sqrt{1 - \frac{r^2}{(L_z - L_r)^2}}. \tag{7.3}$$

We set $\rho = \frac{r}{L_z - L_r}$. We also consider a Taylor expansion of this formula, which is valid for small ρ:

$$\cos\theta = \sqrt{1-\rho^2} \approx 1 - \rho^2/2 \tag{7.4}$$

If r can be written as a function of φ, which requires $\varphi(t)$ to be one-to-one, then

$$\int_0^{\tilde{\tau}} M_\varphi \frac{d\varphi}{dt} dt = \int_0^{2\pi} M_\varphi d\varphi \tag{7.5}$$

With these considerations made, we are ready to evaluate the connection for specific trajectories.

7.2. Circle centred

A circle is straightforward to analyse here, since the radius and thus integrand don't change. We say

$$\rho(\varphi) = R \tag{7.6}$$

and so components of the integral in (7.5) can be evaluated:

$$\int_0^{2\pi} \cos\theta d\varphi = 2\pi\cos\theta = 2\pi\sqrt{1-R^2}. \tag{7.7}$$

7.3. Circle not enclosing centre

Now we would like to know what happens when the trajectory is not in the middle of the disc. We take a circle just next to the origin to compare, because this has an elegant form, but this also turns out to give an interesting result. The describing equation is

$$\rho(\varphi) = 2R\cos\varphi, \tag{7.8}$$

where $\varphi = -\pi/2 \ldots \pi/2$. This gives the integral

$$\delta = \int_{-\pi/2}^{\pi/2} \cos\theta d\varphi = 2\int_{0}^{\pi/2} \cos\theta d\varphi = 2\int_{0}^{\pi/2} \sqrt{1-4R^2\cos^2\varphi} d\varphi, \tag{7.9}$$

where the symmetry of $\cos(\varphi)$ was used. We rewrite as an elliptic integral of the second kind, which is given by $E(\varphi|k^2) = \int_0^{\varphi} \sqrt{1+k^2\sin^2 x}\, dx$:

$$\delta = 2\sqrt{1-4R^2}\int_0^{\pi/2} \sqrt{1+\frac{4R^2}{1-4R^2}\sin^2\varphi} d\varphi = 2\sqrt{1-4R^2}E\left(\sqrt{\frac{4R^2}{1-4R^2}}\right), \tag{7.10}$$

where $E(k) = E(\pi/2|k^2)$ is the complete elliptic integral of the second kind.

If we use our approximation (7.4) the integral reads

$$\delta \approx 2\int_0^{\pi/2} \cos\theta d\varphi = 2\int_0^{\pi/2} 1-2R^2\cos^2\varphi d\varphi = \pi(1-R^2). \tag{7.11}$$

This shows an interesting difference compared to the regular circle, namely that the angle for vanishing radius is π which is twice as small. This is not surprising as the range of φ and therefore of the integral is also only half a round here. So it is clear that the rotation angle in parameter space is very significant for the rotation angle on the Bloch sphere.

7.4. Ellipse

The polar equation of an ellipse around the origin is

$$\rho(\varphi) = \frac{b}{\sqrt{1-(e\cos\varphi)^2}}, \tag{7.12}$$

where $e = \sqrt{1-(b/a)^2}$ is the eccentricity. The integral (7.5) in this case is

$$\delta = \int_0^{2\pi} \cos\theta d\varphi = \int_0^{2\pi} \sqrt{1-\frac{b^2}{1-(e\cos\varphi)^2}} d\varphi. \tag{7.13}$$

We further rewrite making the substitution $x = e\cos\varphi$ to change variable convert into another possible form

$$\delta = 4\int_0^{\pi/2} \sqrt{\frac{1-b^2-(e\cos\varphi)^2}{1-(e\cos\varphi)^2}} d\varphi = -\frac{4}{e}\int_0^1 \sqrt{\frac{1-b^2-x^2}{(1-e^{-2}x^2)(1-x^2)}} dx, \tag{7.14}$$

where we have used that the integrand is periodic with period π and is symmetric around $\phi = \pi/2$ to divide the domain of integration into 4 equal parts.

This seems not to be solvable algebraically in general, but one might consider special cases where simultaneously $b = 0 \wedge e = 1$, or $b = 1$ or $e = 1 \wedge b \neq 0$. The first holds in the limit of very small semi-minor axis b compared to $L_z - L_r$ and semi-major axis a and simplifies the first integral in (7.14) to -2π. For the second situation $b = 1$ we get

$$\delta = 4e\int_0^{\pi/2} \frac{1}{\sqrt{1-(e\cos\varphi)^2}} \cos\varphi d\varphi = \frac{4e}{\sqrt{1-e^2}}\int_0^{\pi/2} \frac{\cos\varphi}{\sqrt{1+\frac{e^2}{1-e^2}\sin^2\varphi}} d\varphi. \tag{7.15}$$

This is similar to an elliptic integral of the second kind and a solution exists given by

$$\delta = 4\left[\arcsin\left(\frac{e}{\sqrt{1-e^2}}\sin x\right)\right]_0^{\pi/2} = 4\arcsin\left(\frac{e}{\sqrt{1-e^2}}\right). \tag{7.16}$$

Finally, $e = 1$ corresponds to a very large semi-major axis a and is perhaps not very realistic, also if this assumption is made, then the result is

$$\delta = 4\int_0^{\pi/2}\sqrt{\frac{\sin^2\varphi - b^2}{\sin^2\varphi}}d\varphi = 4\int_0^{\pi/2}\sqrt{1-\frac{b^2}{\sin^2\varphi}}d\varphi = 4bi\int_0^{\pi/2}\frac{\sqrt{1-b^{-2}\sin^2\varphi}}{\sin\varphi}d\varphi. \tag{7.17}$$

This integral diverges similarly to $\int dx/x$, as one might expect for large semi-major axis, which is not very useful for our purpose.

The Taylor series approximation (7.4) simplifies the general integral considerably and results in

$$\begin{aligned}\delta &\approx \int_0^{2\pi} 1 - \frac{b^2}{2-2(e\cos\varphi)^2}d\varphi = 2\pi - \frac{b^2}{2}\int_0^{2\pi}\frac{1}{1-e^2\cos^2\varphi}d\varphi \\ &= 2\pi - 4\cdot\frac{b^2}{2\sqrt{1-e^2}}\arctan\left(\frac{\tan(\varphi)}{\sqrt{1-e^2}}\right)\Bigg|_0^{\pi/2} = 2\pi\left(1-\frac{b^2}{2\sqrt{1-e^2}}\right).\end{aligned} \tag{7.18}$$

7.5. Square

The parametrisation of one side of the square is

$$x(t) = R, \qquad y(t) = Rt \tag{7.19}$$

for $t = -1 \ldots 1$, or in polar form

$$\rho(t) = R\sqrt{1+t^2}, \qquad \tan\varphi(t) = t \tag{7.20}$$

in the same time domain. We express again ρ in φ:

$$\rho(\varphi) = R\sqrt{1+\tan^2\varphi} = \frac{R}{|\cos\varphi|}, \tag{7.21}$$

where $\varphi = -\pi/4 \ldots \pi/4$. We can consider only this quarter and multiply by four by symmetry. This gives the integral

$$\delta = 4\int_{-\pi/4}^{\pi/4}\cos\theta d\varphi = 4\int_{-\pi/4}^{\pi/4}\sqrt{1-\frac{R^2}{\cos^2\varphi}}d\varphi. \tag{7.22}$$

We convert our expression to something similar to an elliptic integral of the second kind

$$\delta = 4\int_{-\pi/4}^{\pi/4}\frac{1}{\cos\varphi}\sqrt{1-R^2-\sin^2\varphi}d\varphi = 4\sqrt{1-R^2}\int_{-\pi/4}^{\pi/4}\frac{1}{\cos\varphi}\sqrt{1-\frac{1}{1-R^2}\sin^2\varphi}d\varphi. \tag{7.23}$$

This integral has been solved and the solution is

$$\begin{aligned}\delta &= 2R\ln\frac{\sqrt{1-\frac{1}{1-R^2}\sin^2\varphi} + \sqrt{\frac{R^2}{1-R^2}}\sin(\phi)}{\sqrt{1-\frac{1}{1-R^2}\sin^2\varphi} - \sqrt{\frac{R^2}{1-R^2}}\sin(\phi)} + 4\arcsin\left(\sqrt{\frac{1}{1-R^2}}\sin\varphi\right)\Bigg|_{-\pi/4}^{\pi/4} \\ &= 4R\ln\frac{\sqrt{\frac{1}{R^2}-2}+1}{\sqrt{\frac{1}{R^2}-2}-1} + 4\arcsin\left(\frac{1}{\sqrt{2-2R^2}}\right).\end{aligned} \tag{7.24}$$

Approximating again the integrand using (7.4) greatly simplifies the expression. We have

$$\delta \approx 4\int_{-\pi/4}^{\pi/4} \cos\theta d\varphi = 4\int_{-\pi/4}^{\pi/4} 1 - \frac{R^2}{2\cos^2\varphi} d\varphi = 2\pi - 2R^2\left[\tan\varphi\right]_{-\pi/4}^{\pi/4} = 2\pi - 4R^2. \tag{7.25}$$

The result is comparable to that of the circle in (7.7).

7.6. Comparison

We see in figure 7.1 that our quasi-classical approximations seem valid and the calculated connection for the circle closely resembles the numerical result of chapter 5 in the limit of large capacity. Capacities larger than $C = 20$ are not considered, because convergence is not guaranteed. The slope, particularly for small radius, is almost the same. A difference is the value at zero area present for the numerics. This is probably not caused by the number of basis states used, since figure 5.4 does not converge to zero at the beginning, but it might be explained by the fact that a very small offset from the disc was used. For large radius the quasi-classical line diverges, however, for these values the wavefunctions would overlap and the approximations no longer hold.

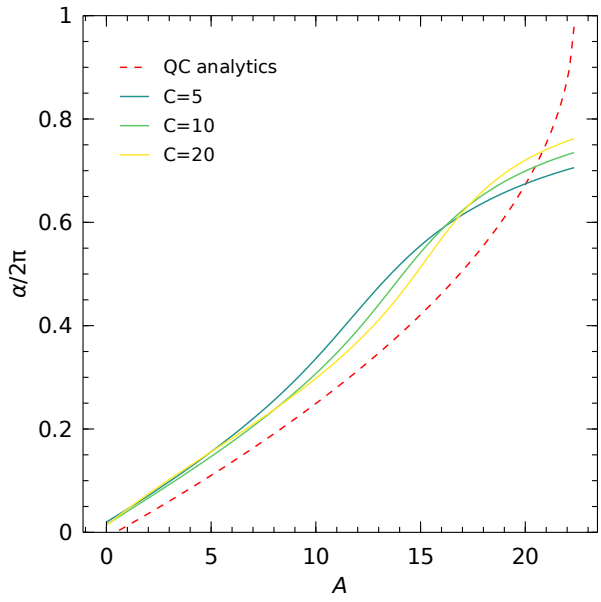

Figure 7.1: The geometric phase for traversing one circle as function of the enclosed area for exact treatment and for the quasi-classical approach. The lines with capacities are of course from the exact formulas. The results in quasi-classical approximations show very good agreement with numerics for small area. The slope is correct, but there is a difference in offset, perhaps as a result of the small offset in the earlier numerics. (The number of harmonic basis functions used is 20^3. Parameters: $L_z = 4, L_r = 4/3, l_n = 1$.)

For each of the trajectories geometric phase has been calculated as function of enclosed area (measured in the disc plane). The result is in figure 7.2. The behaviour seems to be independent of shape, as for small area they all have the same linear behaviour. The endpoints of the graphs is where the minima/wavefunctions would meet on the disc. The ellipse and square reach this point earlier than the circle and this is why they should also diverge earlier, as confirmed in the plot. This result confirms that the parametric fluctuations won't influence the acquired phase much.

Figure 7.2 also shows a circle not enclosing the centre has almost no geometric phase. This shows that for a geometric phase the disc centre needs to be enclosed. We have also done calculations for translated enclosing circles, but as soon as the disc centre is in the circle the line is the same as for the regular circle (for small area), again proving robustness against parametric fluctuations. The line for a circle through the disc centre is in between.

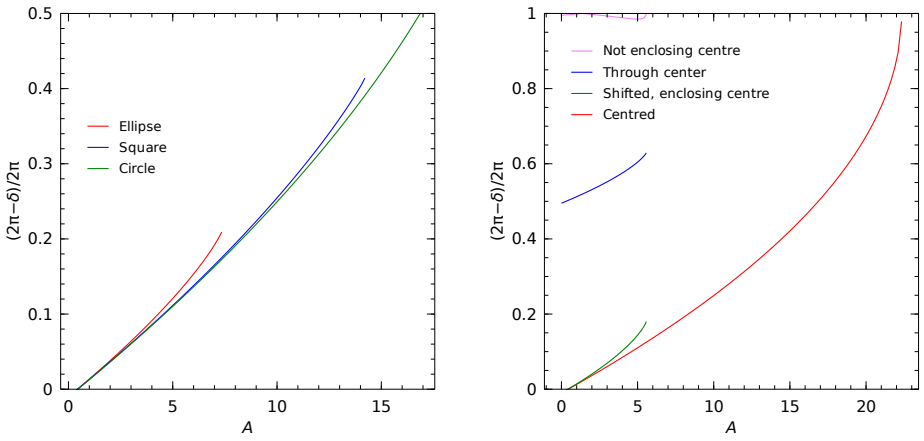

Figure 7.2: The rotation angle on the Bloch Sphere for traversing one cycle on different trajectories as function of the enclosed area. The endpoints is where the minima meet. *Left*: Different shapes (eqs. (7.7), (7.14), (7.24)) *Right*: Shifted circles, i.e. the same radius but with the disc centre on it's edge or inside/outside by $R \cdot 10^{-6}$, where R is the radius. For small area the system is insensitive to shape and so to noise and we get a geometric phase as long as the disc centre is enclosed. (Parameters: $L_z = 4, L_r = 4/3, I_n = 1$, eccentricity of the ellipse $e = 0.94$.)

8

Conclusion

We have considered the quasi-classical regime and the adiabatic limit and have shown the Weyl disk quantum system can undergo cyclic evolution in a degenerate space and we could use this to perform holonomic computation.

This is proved by finding the evolution operator and the connection for going round on a circle on isotropic disc. We have shown that the σ_z operator represents the connection.

We have characterised in a numerical assessment the behaviour of our qubit. We have shown that we have wavefunctions that are localized and separated and approach each other, when moving away from the centre of the disc. They follow the double-well potential minima. The corresponding spins are seen to follow the opposite directions of the minima and accordingly the geometric phase can be tuned, since it determines the connection. We have restricted the capacitiy value, because the dimensions of the Hilbert space needed to accurately represent our states increases with capacity. However, the quasi-classical behaviour for used capacities is confirmed by the results. The states in the upper and lower minimum have turned out to be cyclic and get a geometric phase which increases for larger radius.

Subsequently we have made some approximations valid for small area in the quasi-classical limit, to then calculate the connection for moving in radial and tangential direction. With these we are able to calculate the evolution for any trajectory by parametrising it. Only the tangential direction has non-zero connection and results in a phase to the states, as before.

We have done calculations for circular, square and elliptical trajectories. We have shown that as long as the trajectory encompasses the centre of the disc, there is a geometric phase only determined by the enclosed area. We proved the form of the trajectory doesn't affect the geometric phase to first order. This indicates the desired insensitivity to noise expected from holonomic computation. Our quasi-classical approach agrees very well with the general numerics for the quasi-classical regime, as can be seen by the slope for small area in the plots of the geometric phase.

The results of this thesis show that a geometric phase can be aqcuired by moving around the disc centre and that it is tunable by the enclosed area. What is left is reaching the qubit to read it out and initialise it to a desired state. A previous paper about an Andreev qubit [17] has succesfully done this on a comparable systemfor non-degenerate levels. We can split our levels by bringing the phase out of the disc in the easy direction or radially. In the first case the system provides levels in each minima, in the latter case it provides an even and an odd eigenstate for moderate radius or a ground and excited harmonic eigenstate for large radius. These bases could allow for a variety of manipulations, but it is not yet thoroughly investigated how one could perform general computation.

9

Appendix

9.1. Evolution operator

The Schrödinger equation for the Weyl disk can solved in adiabatic approximation by considering our wave function as the sum of time-dependent eigenfunctions with time-dependent coefficients.

$$\begin{aligned} i\,|\dot{\psi}(t)\rangle &= H(t)\,|\psi(t)\rangle \\ |\psi(t)\rangle &= c_+(t)\,|+(t)\rangle + c_-(t)\,|-(t)\rangle\,. \end{aligned} \tag{9.1}$$

Degeneracy is taken into account by saying

$$\begin{aligned} H(t)\,|+(t)\rangle &= 0 \\ H(t)\,|-(t)\rangle &= 0. \end{aligned} \tag{9.2}$$

We are free to choose a reference energy and have set the energies to zero. With this equation (9.1) becomes

$$\dot{c}_+(t)\,|+(t)\rangle + \dot{c}_-(t)\,|-(t)\rangle + c_+(t)\,|\dot{+}(t)\rangle + c_-(t)\,|\dot{-}(t)\rangle = 0.$$

Letting the operators $\langle\pm(t)|$ work from the left this can be transformed into

$$\begin{aligned} \dot{\vec{c}} &= -M\vec{c} \\ \vec{c} &= \begin{bmatrix} c_+ \\ c_- \end{bmatrix} \\ M &= \begin{bmatrix} \langle+|\dot{+}\rangle & \langle+|\dot{-}\rangle \\ \langle-|\dot{+}\rangle & \langle-|\dot{-}\rangle \end{bmatrix}. \end{aligned} \tag{9.3}$$

This is a very simple differential equation and the solution is

$$\vec{c}(t) = e^{-\int M dt}\vec{c}(0). \tag{9.4}$$

So we have our evolution operator

$$U(t) = e^{-\int M dt} \tag{9.5}$$

and recognise the 2×2 connection $-M$ for this case.

There is a problem with our formulation above. We have not well defined our states $|+(t)\rangle, |-(t)\rangle$, which are (normalised) eigenstates of our Hamiltonian at any time and so are only defined up to a complex phase. What is important for the choice of phase is that the derivatives involved exist and that for the calculation of the evolution over a cycle the initial and final eigenvectors are the same, so the phase of the evolution operator is correct.

9.2. A formula for L_z

We derive here the representation of the operator $\hat{L}_z$ in the harmonic oscillator basis:

$$Y(x,y) = Y_{mn}\psi_{mn}(x,y) = Y_{mn}F_m(x)F_n(y) \tag{9.6}$$

where $F_m(x) = \frac{\sqrt{\alpha}}{2\sqrt{2^n n!}\sqrt[4]{\pi}} e^{-\alpha^2 x^2/2} H_n(\alpha x)$ are harmonic oscillator eigenfunctions and $(Rx, Ry) = (x\cos\theta - y\sin\theta, y\cos\theta + x\sin\theta)$. Recall that

$$i\hat{L}_z = \left.\frac{\partial \tilde{U}(R)}{\partial\theta}\right|_{\theta=0} \tag{9.7}$$

and

$$\tilde{U}(R)Y(x,y) = Y_{mn}F_m(Rx)F_n(Ry) \tag{9.8}$$

Then the matrix elemwnt of $\tilde{U}$ is

$$\tilde{U}(R)_{m'n',mn} = \langle\psi_{mn}(x,y)|\tilde{U}(R)|\psi_{m'n'}(x,y)\rangle = \int F_m(Rx)F_n(Ry)F_{m'}F_{n'}dxdy \tag{9.9}$$

Now we can extract the matrix elements from this. We take the derivative of (9.9)

$$\frac{d\tilde{U}(R)_{m'n',mn}}{d\theta} = \int \frac{d}{d\theta}\left[F_m(Rx)F_n(Ry)\right]F_{m'}F_{n'}dxdy \tag{9.10}$$

and then calculate derivatives of the harmonics

$$\begin{aligned}\frac{d}{d\theta}\left[F_m(Rx)F_n(Ry)\right] &= \frac{dRx}{d\theta}F_m'(Rx)F_n(Ry) + \frac{dRy}{d\theta}F_m(Rx)F_n'(Ry)\\ &= (-x\sin\theta - y\cos\theta)F_m'(Rx)F_n(Ry)\\ &\quad + (-y\sin\theta + x\cos\theta)F_m(Rx)F_n'(Ry).\end{aligned} \tag{9.11}$$

Taking the value at zero angle yields

$$\left.\frac{d}{d\theta}\right|_{\theta=0}\left[F_m(Rx)F_n(Ry)\right] = -yF_m'(Rx)F_n(Ry) + xF_m(Rx)F_n'(Ry). \tag{9.12}$$

The end result is

$$i\hat{L}_{z,m'n'mn} = \int xF_m(x)F_{m'}(x)dx\int F_n'(y)F_{n'}(y)dy - \int F_m'(x)F_{m'}(x)dx\int yF_n(y)F_{n'}(y)dy, \tag{9.13}$$

but we can simplify this into

$$\begin{aligned}i\hat{L}_{z,m'n'mn} &= F_{mm'}D_{nn'} - D_{mm'}F_{nn'}\\ F_{mn} &= \int xF_m(x)F_n(x)dx\\ D_{mn} &= \int F_m'(x)F_n(x)dx.\end{aligned} \tag{9.14}$$

In our case the two levels of interest are close to the same oscillator state $Y(\phi_x,\phi_z) = F(\phi_x - \phi_x^0)F(\phi_z \pm \phi_z^0)$ with different spin and shifted by the reservoir phases. It turns out $\hat{L}_z$ doesn't couple between these two states. To prove this consider the following two properties of Hermite polynomials:

$$H_n' = 2nH_{n-1} \tag{9.15}$$

and

$$\begin{aligned}xH_n &= \frac{1}{2}H_{n+1} + \frac{1}{2}H_n'\\ &= \frac{1}{2}H_{n+1} + nH_{n-1}.\end{aligned} \tag{9.16}$$

This allows F_{nn}, D_{nn} to be rewritten to only contain harmonic oscillator functions. Since

$$xF_n = \sqrt{\frac{n+1}{2}}F_{n+1} + \sqrt{\frac{n}{2}}F_{n-1} \tag{9.17}$$

we have

$$F_{nn} = \int xF_n(x)F_n(x)dx = 0 \tag{9.18}$$

and since

$$\begin{aligned} F_n' &= -xF_n + \sqrt{2n}F_{n-1} \\ &= \sqrt{\frac{n}{2}}F_{n-1} - \sqrt{\frac{n+1}{2}}F_{n+1} \end{aligned} \tag{9.19}$$

we have also

$$D_{nn} = \int F_n'(x)F_n(x)dx = 0. \tag{9.20}$$

The shift in coordinates clearly doesn't change this result, so $\hat{L}_z$ only couples between "neighbouring" oscillator states. This means that only σ_z in A in (4.13) contributes to matrix M.

9.3. Moore's derivation that $U(t) = e^{-iAt}e^{-iBt}$

For Hamiltonians of the special form

$$H(t) = e^{-iAt}\tilde{H}e^{iAt}, \tag{9.21}$$

where $\tilde{H}$ and A are time independent, it can be shown by direct substitution into the Schrödinger equation that the evolution operator is given by

$$U(t) = e^{-iAt}e^{-iBt}, \tag{9.22}$$

where $B = \tilde{H} - A$ [31]. If also the Hamiltonian is periodic $H(\tilde{t}) = H(0)$, the operators B and $e^{-iA\tilde{t}}$ commute and must have the same eigenstates.

$$\begin{aligned} B\phi_\alpha &= B_\alpha\phi_\alpha \\ e^{-iA\tilde{t}}\phi_\alpha &= e^{-i\theta_\alpha}\phi_\alpha \end{aligned} \tag{9.23}$$

This means that these eigenstates are cyclic states of the Hamiltonian, states which return to their initial states after one period.

$$U(\tilde{t})\phi_\alpha = e^{-i\theta_\alpha}e^{-iB_\alpha\tilde{t}}\phi_\alpha \tag{9.24}$$

So the cyclic states get a phase $-\theta_\alpha - B_\alpha\tilde{t}$ for each cycle, which can be separated into a Berry phase and a dynamical phase. The dynamical part can be evaluated by

$$\begin{aligned} \delta_\alpha &= -\int_0^{\tilde{t}} \langle\phi_\alpha|U^*(t)H(t)U(t)|\phi_\alpha\rangle\, dt \\ &= -B_\alpha\tilde{t} - \langle\phi_\alpha|A|\phi_\alpha\rangle\,\tilde{t} \end{aligned} \tag{9.25}$$

and the geometric part is just the difference

$$\gamma_\alpha = \langle\phi_\alpha|A|\phi_\alpha\rangle\,\tilde{t} - \theta_\alpha. \tag{9.26}$$

9.3.1. Weyl disk system

The Hamiltonian of our system is of the form (9.21), so the above results apply. The situation is somewhat simpler, because in our case $e^{-iA\tilde{t}} = e^{-i.2\pi\sigma_z} = 1$ so $\theta_\alpha = 0$ and because the rotation speed is considered large enough ($\omega \ll \Delta$) such that the dynamical phase is negligible and only the Berry phase $\gamma_\alpha = \langle\phi_\alpha|A|\phi_\alpha\rangle\,\tilde{t}$ remains. This means that in the cyclic basis

$$\begin{aligned} U(\tilde{t}) &= \begin{bmatrix} e^{i\langle\phi_+|\sigma_z|\phi_+\rangle\tilde{t}} & 0 \\ 0 & e^{i\langle\phi_-|\sigma_z|\phi_-\rangle\tilde{t}} \end{bmatrix} \\ &= e^{i\sigma_z\tilde{t}}, \end{aligned} \tag{9.27}$$

where we have used that the states do not overlap in coordinate space. This corresponds to $M = -i\omega\sigma_z/2$ in (2.8).

9.4. Code

The code for the calculations and numerics is written in Julia and can be executed from https://gitlab.tudelft.nl/jerdmani where further instructions are given.

Bibliography

[1] Feynman, R. (1982). Simulating physics with computers. International Journal of Theoretical Physics, 21(6-7), pp.467-488.

[2] Shor, P. (1997). Polynomial-Time Algorithms for Prime Factorization and Discrete Logarithms on a Quantum Computer. SIAM Journal on Computing, 26(5), pp.1484-1509.

[3] Bernien, H., Schwartz, S., Keesling, A., Levine, H., Omran, A., Pichler, H., Choi, S., Zibrov, A., Endres, M., Greiner, M., Vuletić, V. and Lukin, M. (2017). Probing many-body dynamics on a 51-atom quantum simulator. Nature, 551(7682), pp.579-584.

[4] http://akyrillidis.github.io/notes/quant_post_7

[5] Nazarov, Y. and Blanter, Y. (2009). Quantum Transport: Introduction to Nanoscience. Cambridge University Press.

[6] Lee Gomes (2018). Quantum Computers Strive to Break Out of the Lab. https://spectrum.ieee.org/computing/hardware/quantum-computers-strive-to-break-out-of-the-lab

[7] Bommer, J., Zhang, H., Gül, Ö., Nijholt, B., Wimmer, M., Rybakov, F., Garaud, J., Rodic, D., Babaev, E., Troyer, M., Car, D., Plissard, S., Bakkers, E., Watanabe, K., Taniguchi, T. and Kouwenhoven, L. (2019). Spin-Orbit Protection of Induced Superconductivity in Majorana Nanowires. Physical Review Letters, 122(18).

[8] Philip Ball (2018). https://physicsworld.com/a/ion-based-commercial-quantum-computer-is-a-first/

[9] R. Colin Johnson (2019). https://cacm.acm.org/news/236266-worlds-largest-quantum-computer-doubles-down/fulltext

[10] https://www.xanadu.ai/hardware/

[11] Wecker, D., Hastings, M., Wiebe, N., Clark, B., Nayak, C. and Troyer, M. (2015). Solving strongly correlated electron models on a quantum computer. Physical Review A, 92(6).

[12] Wecker, D., Bauer, B., Clark, B., Hastings, M. and Troyer, M. (2014). Gate-count estimates for performing quantum chemistry on small quantum computers. Physical Review A, 90(2).

[13] Jordan, S., Lee, K. and Preskill, J. (2012). Quantum Algorithms for Quantum Field Theories. Science, 336(6085), pp.1130-1133.

[14] Zhang, J., Pagano, G., Hess, P., Kyprianidis, A., Becker, P., Kaplan, H., Gorshkov, A., Gong, Z. and Monroe, C. (2017). Observation of a many-body dynamical phase transition with a 53-qubit quantum simulator. Nature, 551(7682), pp.601-604.

[15] Zazunov, A., Shumeiko, V., Bratus', E., Lantz, J. and Wendin, G. (2003). Andreev Level Qubit. Physical Review Letters, 90(8).

[16] Shafranjuk, S., Nevirkovets, I. and Ketterson, J. (2002). A qubit device based on manipulations of Andreev bound states in double-barrier Josephson junctions. Solid State Communications, 121(9-10), pp.457-460.

[17] Janvier, C., Tosi, L., Bretheau, L., Girit, Ç., Stern, M., Bertet, P., Joyez, P., Vion, D., Esteve, D., Goffman, M., Pothier, H. and Urbina, C. (2015). Coherent manipulation of Andreev states in superconducting atomic contacts. Science, 349(6253), pp.1199-1202.

[18] Abdumalikov Jr, A., Fink, J., Juliusson, K., Pechal, M., Berger, S., Wallraff, A. and Filipp, S. (2013). Experimental realization of non-Abelian non-adiabatic geometric gates. Nature, 496(7446), pp.482-485.

[19] Toyoda, K., Uchida, K., Noguchi, A., Haze, S. and Urabe, S. (2013). Realization of holonomic single-qubit operations. Physical Review A, 87(5).

[20] Economou, S. and Reinecke, T. (2007). Theory of Fast Optical Spin Rotation in a Quantum Dot Based on Geometric Phases and Trapped States. Physical Review Letters, 99(21).

[21] Li, H., Liu, Y. and Long, G. (2017). Experimental realization of single-shot nonadiabatic holonomic gates in nuclear spins. Science China Physics, Mechanics & Astronomy, 60(8).

[22] Nagata, K., Kuramitani, K., Sekiguchi, Y. and Kosaka, H. (2018). Universal holonomic quantum gates over geometric spin qubits with polarised microwaves. Nature Communications, 9(1).

[23] Aharonov, Y. and Anandan, J. (1987). Phase change during a cyclic quantum evolution. Physical Review Letters, 58(16), pp.1593-1596.

[24] Nenciu, G. (1980). On the adiabatic theorem of quantum mechanics. Journal of Physics A: Mathematical and General, 13(2), pp.L15-L18.

[25] Quantal phase factors accompanying adiabatic changes. (1984). Proceedings of the Royal Society of London. A. Mathematical and Physical Sciences, 392(1802), pp.45-57.

[26] Carollo, Angelo and Vedral, Vlatko. (2005). Holonomic Quantum Computation.

[27] Berry phase for a spin 1/2 particle in a classical fluctuating field; Gabriele De Chiara, G. Massimo Palma; Phys. Rev. Lett., 91:art. no.–090404, 2003

[28] Zhu, S. and Wang, Z. (2002). Implementation of Universal Quantum Gates Based on Nonadiabatic Geometric Phases. Physical Review Letters, 89(9).

[29] Riwar, R., Houzet, M., Meyer, J. and Nazarov, Y. (2016). Multi-terminal Josephson junctions as topological matter. Nature Communications, 7(1).

[30] Erdmanis, J., Lukács, Á. and Nazarov, Y. (2018). Weyl disks: Theoretical prediction. Physical Review B, 98(24).

[31] Moore, D. (1992). Berry phases and Rabi oscillations. Quantum Optics: Journal of the European Optical Society Part B, 4(2), pp.123-130.

[32] Nielsen, M. and Chuang, I. (2019). Quantum computation and quantum information. Cambridge: Cambridge University Press.